SEDIMENTOLOGY the journal of the International Association of Sedimentologists

Sedimentology (2020) **67**, 118–151 doi: 10.1111/sed.12637

Application of sequence stratigraphic concepts to the Upper Cretaceous Tununk Shale Member of the Mancos Shale Formation, south-central Utah: Parasequence styles in shelfal mudstone strata

ZHIYANG LI and JUERGEN SCHIEBER
Department of Earth and Atmospheric Sciences, Indiana University Bloomington, 1001 East 10th Street, Bloomington, Indiana, 47405, USA (E-mail: zl29@iu.edu)

Associate Editor – Massimiliano Ghinassi

ABSTRACT

Although sequence stratigraphic concepts have been applied extensively to coarse-grained siliciclastic deposits in nearshore environments, high-resolution sequence stratigraphic analysis has not been widely applied to mudstone-dominated sedimentary successions deposited in more distal hemipelagic to pelagic settings. To examine how sequence stratigraphic frameworks can be derived from the facies variability of mudstone-dominated successions, the Tununk Shale Member of the Mancos Shale Formation in south-central Utah (USA) was examined in detail through a combination of sedimentological, stratigraphic and petrographic methods. The Tununk Shale accumulated on a storm-dominated shelf during the second-order Greenhorn sea-level cycle. During this eustatic event, the depositional environment of the Tununk Shale shifted laterally from distal middle shelf to outer shelf, then from an outer shelf to an inner shelf environment. At least 49 parasequences can be identified within the Tununk Shale. Each parasequence shows a coarsening-upward trend via upward increases in silt and sand content, thickness and lateral continuity of laminae/beds, and abundance of storm-generated sedimentary structures. Variations in bioturbation styles within parasequences are complex, although abrupt changes in bioturbation intensity or diversity commonly occur across parasequence boundaries (i.e. flooding surfaces). Due to changes in depositional environments, dominant sediment supply and bioturbation characteristics, parasequence styles in the Tununk Shale show considerable variability. Based on parasequence stacking patterns, eleven system tracts, four depositional sequences and key sequence stratigraphic surfaces can be identified. The high-resolution sequence stratigraphic framework of the Tununk Shale reveals a hierarchy of stratal cyclicity. Application of sequence stratigraphic concepts to this thick mudstone-dominated succession provides important insights into the underlying causes of heterogeneity in these rocks over multiple thickness scales (millimetre-scale to metre-scale). The detailed sedimentological characterization of parasequences, system tracts and depositional sequences in the Tununk Shale provides conceptual approaches that can aid the development of high-resolution sequence stratigraphic frameworks in other ancient shelf mudstone successions.

Keywords Mudstone facies, mudstone petrography, sequence stratigraphy, storm-dominated shelf, Tununk Shale, Turonian, Western Interior Seaway.

INTRODUCTION

Sequence stratigraphy is the study of rock relationships within a time-stratigraphic framework of repetitive, genetically related strata bounded by surfaces of erosion or non-deposition, or their correlative conformities (Posamentier *et al.*, 1988; Van Wagoner *et al.*, 1988, 1990). This framework ties changes in stratal stacking patterns developed in response to variations in sediment supply and accommodation and provides the context within which evolution of depositional systems through space and time can be interpreted (Jervey, 1988; Posamentier & Allen, 1999; Catuneanu *et al.*, 2009, 2011). Since the concepts of sequence stratigraphy were proposed in the 1970s, sequence stratigraphic methods have been widely applied to coarse-grained siliciclastic deposits in coastal and shallow-marine environments, owing to the potential of these rocks to form significant hydrocarbon reservoirs (e.g. Van Wagoner *et al.*, 1990; Catuneanu *et al.*, 2009). Because nearshore environments are sensitive to relative changes in sea level, sediments deposited in these environments are particularly suitable for high-resolution sequence stratigraphic analysis (Catuneanu *et al.*, 2009; Reynolds, 2009).

Fine-grained sedimentary rocks (i.e. mudstones/shales that are composed mainly of particles smaller than 62.5 μm) constitute approximately two-thirds of the sedimentary rock record (Potter *et al.*, 2005; Lazar *et al.*, 2015), and they can serve as petroleum source rocks, unconventional hydrocarbon reservoirs and seals. In spite of the great economic significance of these rocks, high-resolution sequence stratigraphic analysis has seldom been attempted in mudstone-dominated successions deposited in more distal settings (for example, hemipelagic to pelagic) (e.g. Bohacs & Schwalbach, 1992; Bohacs, 1998; Macquaker *et al.*, 1998, 2007; Schieber, 1998a). This state of affairs is due to the inherent difficulties that complicate detailed facies analysis of mudstones, such as susceptibility to weathering and largely cryptic variability in grain size and sedimentary features. Yet, notwithstanding these obstacles, a comprehensive understanding of sedimentary facies and their associations is essential for reliable interpretations of stacking patterns and sequence stratigraphic surfaces (Catuneanu, 2006). Nonetheless, many investigations of facies variability in fine-grained sedimentary successions rely heavily on data from mineralogical, geochemical, or palaeontological analyses (e.g. Ver Straeten *et al.*, 2011; Ayranci *et al.*, 2018), even though key information such as grain size, sedimentary textures, biogenic features and origin of different components cannot be directly obtained with these techniques (Macquaker *et al.*, 2007).

Recent advances in flume experiments on mud transport and deposition (Schieber *et al.*, 2007; Schieber & Southard, 2009; Schieber, 2011), as well as observations on modern muddy shelves (Rine & Ginsburg, 1985; Kuehl *et al.*, 1986; Nittrouer *et al.*, 1986; Wright *et al.*, 1988; Kineke *et al.*, 1996; Allison *et al.*, 2000; Traykovski *et al.*, 2000), have shown that the processes responsible for mud deposition and formation of fine-grained sedimentary successions are much more dynamic than traditionally presumed. A growing number of case studies of ancient fine-grained sedimentary successions also show that mudstone successions, albeit appearing homogeneous in outcrops or cores, are characterized by small-scale cyclic facies variations (i.e. parasequences and parasequence sets) when examined in detail (Bohacs & Schwalbach, 1992; Macquaker *et al.*, 1996, 1998, 2007; Macquaker & Taylor, 1996; Bohacs, 1998; Schieber, 1998a; Macquaker & Howell, 1999; Bohacs *et al.*, 2005, 2014; Birgenheier *et al.*, 2017; Wilson & Schieber, 2017). Their recognition poses the question as to what are the dominant processes that produce the complex variability observed in mudstones, and control the evolution of mud-dominated systems through space and time. To date, owing to the paucity of published studies of mudstone successions that have been comprehensively evaluated with sequence stratigraphic methods, many of these important questions remain unresolved.

For this study, the extensive exposures of the Upper Cretaceous Tununk Shale Member in south-central Utah afford an excellent opportunity to examine small-scale (parasequence-scale) facies variations within this ancient shelf mudstone succession, and enable understanding of the evolution of the depositional system through time and space within a sequence stratigraphic framework. The focus of previous studies of the Tununk Shale was mainly on regional stratigraphy, as well as mineralogical and geochemical characteristics. Chronostratigraphic correlations (bentonite beds) between the Tununk Shale in south-central Utah (Henry Mountains Region) with its lateral equivalent, the Tropic Shale in southern Utah (Kaiparowits Plateau) led to recognition of offshore prograding clinoform

geometries (Leithold, 1994; Sethi & Leithold, 1997; Leithold & Dean, 1998) that were interpreted to indicate a muddy prodeltaic depositional setting. Based on integrated analysis of textures (i.e. grain size) and mineralogy, as many as 37 parasequences and six sequences were identified in the Tununk Shale and the Tropic Shale (Leithold, 1994).

The offshore prograding clinoform geometries documented in Leithold (1994), however, are neither uniquely diagnostic of the dominant sediment-transport mechanism nor of a specific source at the shoreline (a delta), as revealed by studies on prograding mud wedges on modern continental shelves (e.g. Cattaneo *et al.*, 2003, 2007; Liu *et al.*, 2007; Patruno *et al.*, 2015). Based on an integrated analysis of sedimentary facies and bioturbation characteristics, palaeocurrent data and palaeogeography, an alternative depositional model of the Tununk Shale accumulating on a storm-dominated shelf was proposed (Li & Schieber, 2018a). This perspective is supported by the recognition that the dominant sediment dispersal mechanisms were storm-generated offshore-directed currents (across-shelf) and geostrophic currents (along-shelf), as illustrated by typical sedimentary facies and facies successions in the Tununk Shale (Li & Schieber, 2018a). The disparity between this and prior depositional models of the Tununk Shale indicates that the validity of previously described parasequences needs to be re-evaluated, because teasing out parasequences based solely on mineralogy is usually complicated by the fact that these rocks usually are composed of complex components (for example, allochthonous, autochthonous and diagenesis-derived) in varying proportions (Macquaker *et al.*, 2007; Aplin & Macquaker, 2011; Lazar *et al.*, 2015). The recognition of parasequences based on an integrated analysis of variations in mineralogical composition, changes in grain size and sedimentary facies characteristics is clearly preferable (Van Wagoner *et al.*, 1990).

The present study re-evaluated the Tununk Shale in south-central Utah via integrated sedimentological, petrographic and stratigraphic analyses, with the aim to develop a high-resolution sequence stratigraphic framework for this thick ancient shelf mudstone succession. This investigation also serves as a test case for how readily parasequences, system tracts and depositional sequences can be identified in a mudstone-dominated succession. Characteristics of parasequences, system tracts and sequences in the Tununk are described and summarized to this end, to provide a better understanding and guidance for the conduct of sequence-stratigraphic analysis of other shelf mudstone successions in the stratigraphic record.

GEOLOGICAL BACKGROUND

During the Late Jurassic and Cretaceous, the western interior of North America was occupied by an asymmetrical foreland basin that had developed in response to the flexural loading of the Sevier thrust belt (Kauffman, 1977, 1985; Livaccari, 1991; Kauffman & Caldwell, 1993; Liu *et al.*, 2011; DeCelles, 2004). The combined effects of load-induced subsidence and global eustatic highstand throughout the Late Cretaceous resulted in the development of an epicontinental seaway known as the Western Interior Seaway (WIS; Kauffman, 1977, 1985). During the Albian to Maastrichtian, the WIS was subject to five major transgressive–regressive marine cycles with durations from 2 to 10 Myr (Kauffman, 1985); cycles that correspond in duration to second-order cycles, *sensu* Mitchum & Van Wagoner (1991). The most extensive flooding of the seaway occurred during the so-called Greenhorn cycle, when more than one-third of North America was inundated (Fig. 1A). The Greenhorn cycle began in the Late Albian and ended in the Middle Turonian (Kauffman, 1985). During peak transgression in the Early Turonian, the WIS extended from the Arctic Ocean to the Gulf of Mexico and was characterized by a broad shelf (Fig. 1A). The estimated water depth within this epeiric seaway never exceeded more than a few hundred metres water depth (Weimer, 1984; Kauffman, 1985; Sageman & Arthur, 1994). In response to sediments supplied from the unroofing of the Sevier orogenic belt and volcanic highlands to the west, the WIS was broadly characterized by high siliciclastic input and high sedimentation rates along the western margin, and little clastic input on the eastern margin (Kauffman, 1977, 1985; Hart, 2016).

The Upper Cretaceous succession currently exposed in central and southern Utah was deposited along the western margin of the WIS as a series of eastward-prograding clastic wedges (Fig. 1B). Deposition of the Tununk Shale occurred from the Late Cenomanian to the Middle Turonian over a time span of about 2·5 Myr (Zelt, 1985; Leithold, 1994). Driven by the Greenhorn transgressive–regressive sea-level

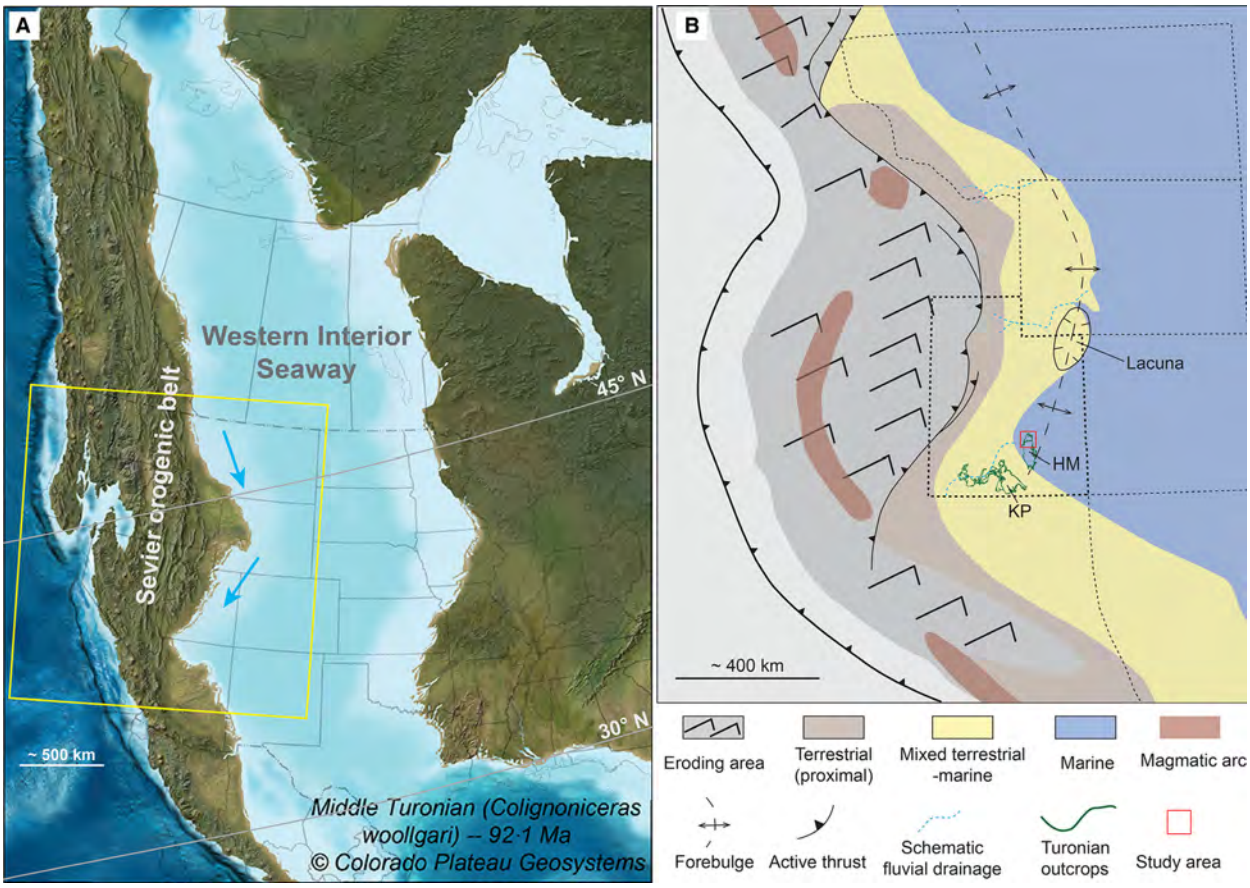

Fig. 1. (A) Middle Turonian palaeogeographic map that shows the extent of the Western Interior Seaway (Blakey, 2014). Dominant southward-directed longshore currents along the western margin of the seaway are indicated by blue arrows. Palaeolatitudes are from Sageman & Arthur (1994). The approximate area of (B) is indicated by the yellow box. (B) Palaeogeographic reconstruction of the foreland basin of middle North America that shows evolving topography (schematic), locations of active faults, general depositional environments, forebulge position during the Turonian and location of the study area (modified from Yonkee & Weil, 2015). The sediment supply of the Tununk Shale was derived from multiple sources, including clastic sediments derived from the Sevier orogenic belt and volcanic highlands to the west, primary productivity from the upper water column, wind-borne volcanic ash, and possibly from submarine erosion at the lacuna developed in north-eastern Utah. The lacuna in north-eastern Utah developed as a submarine unconformity from the Late Cenomanian to Middle Turonian due to the uplift of an intra-basinal culmination (Ryer & Lovekin, 1986). HM: Henry Mountains Region, KP: Kaiparowits Plateau.

cycle, the offshore mudstones of the Tununk Shale overlie the coarser non-marine and paralic deposits of the Dakota Sandstone and grade upward into the shallow marine and deltaic strata of the Ferron Sandstone Member (Fig. 2; Peterson *et al.*, 1980; Kauffman, 1985). During deposition of the Tununk Shale, the palaeoshoreline trended north-east/south-west in the study area (Fig. 1). Although the dominant direction of sediment progradation was eastward, nearshore sediments deposited along the western margin of the WIS were deflected southward by coastal currents generated by a large-scale counterclockwise gyre (Fig. 1; Barron, 1989; Ericksen & Slingerland, 1990; Slingerland & Keen, 1999; Li *et al.*, 2015; Li & Schieber, 2018a).

Depositional framework of the Tununk Shale

In outcrop, the Tununk Shale is an approximately 200 m thick succession that is largely composed of dark grey calcareous to non-calcareous (argillaceous) mudstones with numerous thin silt-rich and sand-rich beds and volcanic ash beds (i.e. bentonites; Peterson

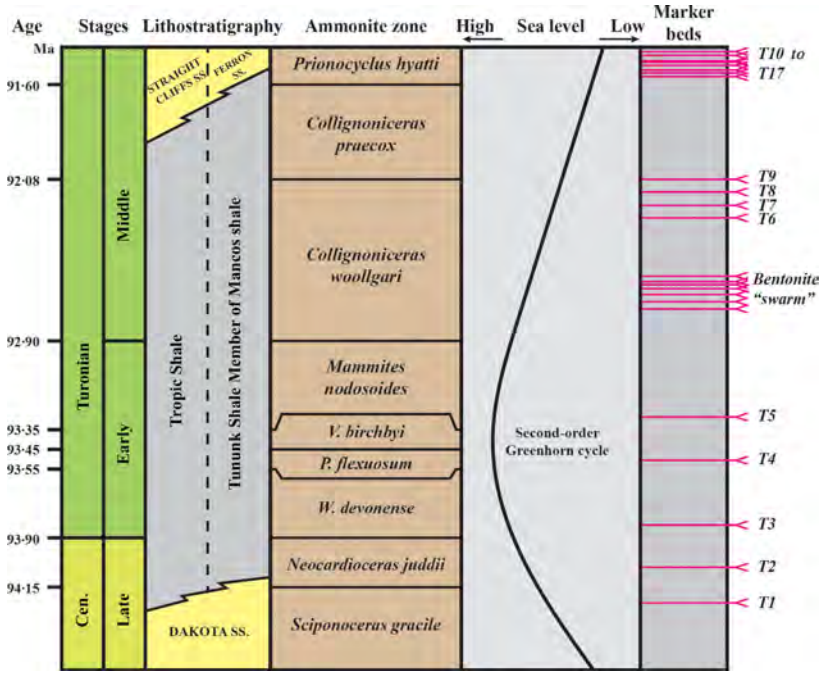

Fig. 2. Lower to Middle Turonian stratigraphy in Southern Utah (compiled from Kauffman, 1977; Zelt, 1985; Leithold, 1994; Leithold & Dean, 1998). Absolute dates are from Ogg *et al.*, 2012.

et al., 1980; Zelt, 1985). In an integrated surface to subsurface study, Zelt (1985) utilized 17 traceable bentonite beds and biostratigraphic relationships to correlate the Tununk Shale in south-central Utah (Henry Mountains Region) with its lateral equivalent, the Tropic Shale in southern Utah (Kaiparowits Plateau; Figs 1B and 2).

Based on an integrated analysis of sedimentary facies and bioturbation characteristics, palaeocurrent data and palaeogeography, the sedimentology and depositional environments of the Tununk Shale are discussed in detail in a previous study (Li & Schieber, 2018a), and are only briefly summarized here. The Tununk Shale ranges in thickness from 170 to 210 m in the study area (Fig. 3) and is interpreted to be accumulated on a storm-dominated shelf. The sediments of the Tununk Shale were derived from multiple sources, including significant amounts of clastic sediments derived from the Sevier orogenic belt and volcanic highlands, primary productivity (for example, foraminifera tests, faecal pellets and coccoliths), wind-borne volcanic ash, and possibly from submarine erosion of the lacuna that had developed in north-eastern Utah (Fig. 1; Li & Schieber, 2018b). Based on the relative proportion between carbonate particles derived from primary productivity versus siliciclastic particles derived from terrigenous input, the Tununk Shale can be divided into four lithofacies packages including: (i) carbonate-bearing (<30% carbonate), silty and sandy mudstone (CSSM); (ii) silt-bearing, calcareous mudstone (SCM, >30% carbonate); (iii) carbonate-bearing, silty mudstone to muddy siltstone (CMS); and (iv) non-calcareous, silty and sandy mudstone (SSM) in an ascending order. Up-section, the relative amount of the carbonate component derived from primary productivity within the Tununk Shale gradually increases from the CSSM to the SCM facies, then decreases to the CMS facies, and becomes absent in the SSM facies. Details of sedimentary and biogenic features in each lithofacies package are summarized in Table 1 and are illustrated using the measured stratigraphic section at Salt Wash (Fig. 4). Vertical variations in lithofacies types and sedimentary facies characteristics indicate that the Tununk Shale shifted laterally from distal middle-shelf to outer-shelf (CSSM to SCM lithofacies), and then back from an outer-shelf to an inner-shelf setting (SCM to CMS, and to SSM lithofacies) (Fig. 4; Table 1). Based on integrated analysis of palaeocurrent data and palaeogeography, storm-induced shore-parallel geostrophic flows and offshore-directed flows likely were the dominant processes that governed the transport and deposition of mud across and along this storm-dominated shelf (Li & Schieber, 2018a).

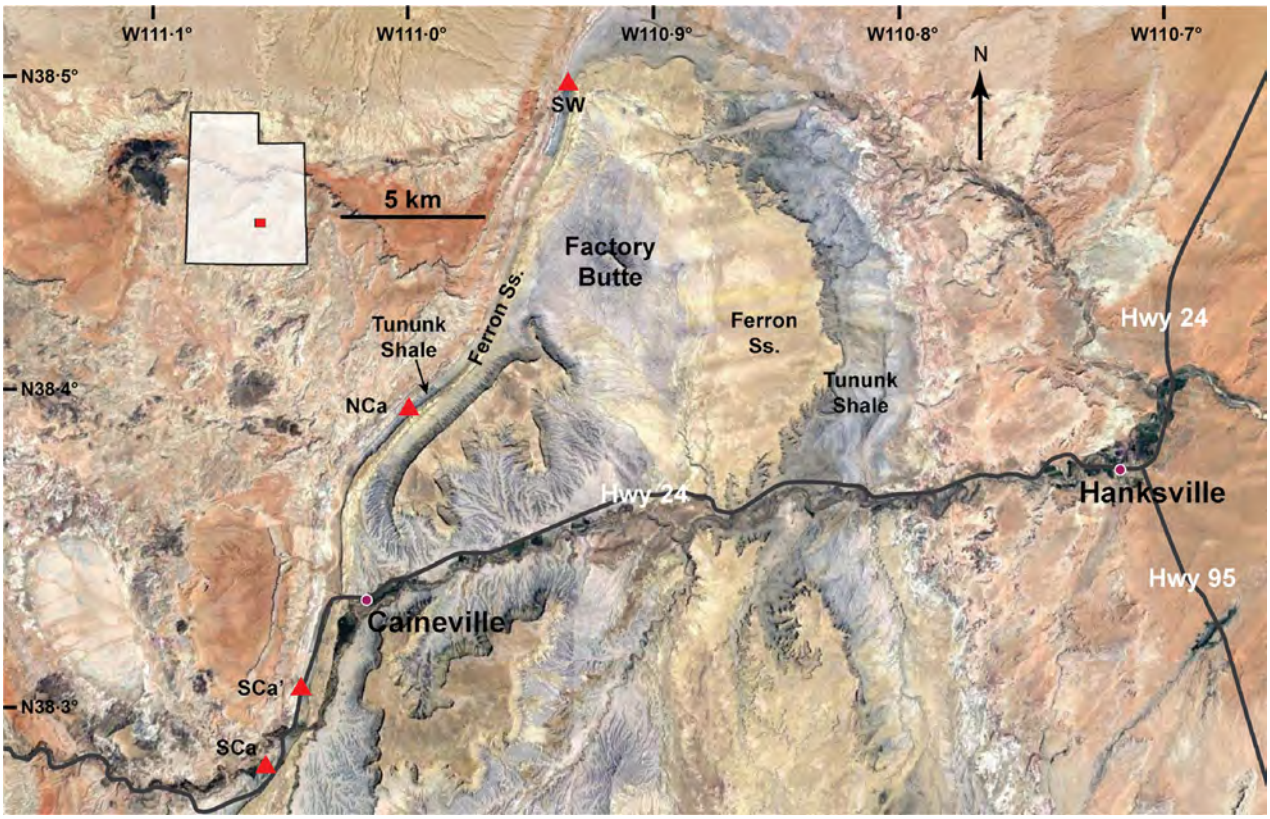

Fig. 3. Map of the Tununk Shale outcrop belts near Hanksville. Red triangles indicate locations of three stratigraphic sections measured in this study (SW: Salt Wash, NCa: North Caineville, and SCa: South Caineville). The section measured at SCa is a composite section consisting of two segments (SCa and SCa′).

METHODS AND TERMINOLOGY FOR SEQUENCE STRATIGRAPHIC ANALYSIS

For this study, the Tununk Shale in the Henry Mountains region of south-central Utah (Fig. 3) was examined to collect data for comprehensive sedimentological and sequence stratigraphic analyses. Three detailed stratigraphic sections near Hanksville, Utah, extending parallel to the palaeoshoreline direction (north-east to south-west), were measured using a Jacob staff (1·5 m long) along a 30 km transect (Fig. 3). Because these rocks are highly susceptible to weathering, steep exposures were chosen and excavated where needed to reveal fresh rock for description and sample collection. For every 1·5 m Jacob staff interval, two small pits (up to several tens of centimetres in both depth and length) were dug in the lower third (0 to 0·5 m) and upper third (1·0 to 1·5 m) intervals to expose fresh rock. Relatively unweathered samples were collected at an average vertical spacing of 1 m (more closely spaced in some places). More than 500 samples, collected from three measured sections, were taken back to the laboratory, embedded in epoxy, slabbed and then polished. High-resolution images of polished slabs were acquired with a flatbed scanner (1200 to 2400 dpi resolution) and then contrast-enhanced in Adobe Photoshop™ to examine small-scale (millimetre-scale to centimetre-scale) sedimentary features and facies variability.

For each stratigraphic section, sedimentological data including lithology, grain size, sedimentary features, bioturbation features, and amount and types of fossil fragments were documented using the methodology of Lazar *et al.* (2015). In the field, grain-size variability was mainly determined by: (i) feeling and chewing rock samples to estimate silt versus clay (i.e. gritty versus smooth) content; and (ii) variations in colour. The relative percentage of silt estimated by chewing essentially mirrors the quartz-silt content and serves as a reliable proxy for grain-size distribution in mudstones that can be related to overall depositional

Table 1. Summary of sedimentary and biogenic features in each lithofacies package within the Tununk Shale (Li & Schieber, 2018a). Four lithofacies packages present in the Tununk Shale include: (i) carbonate-bearing, silty and sandy mudstone (CSSM); (ii) silt-bearing, calcareous mudstone (SCM); (iii) carbonate-bearing, silty mudstone to muddy siltstone (CMS); and (iv) non-calcareous, silty and sandy mudstone (SSM). Combining lithofacies with bioturbation intensity, a total of nine types of 'shale microfacies' (*sensu* Schieber & Zimmerle, 1998) are recognized in the Tununk Shale. These include CSSMm, CSSMh, SCMl, SCMm, CMSm, CMSh, SSMl, SSMm and SSMh (Fig. 5). The lower case letters 'l', 'm' and 'h' following each lithofacies name represent low, medium and high bioturbation intensity, respectively.

Lithofacies	Depositional environment	Degree of clastic dilution	Sedimentary structures	Bioturbation characteristics
CSSM	Distal middle shelf	Moderate to small	Thin (<1 mm to several millimetres) silt to sand lamina to lamina-sets showing starved-ripple cross-lamination (common) and a minor amount of wave ripple cross lamination. Commonly disrupted by burrows	Moderate to high bioturbation intensity (BI = 3–5), low trace-fossil intensity. Ichnogenera present: navichnia (sediment-swimmer traces), *Phycosiphon*, *Chondrites* and rare *Planolites*
SCM	Outer shelf	Small (minimum)	More common and laterally continuous calcareous and silt laminae to lamina-sets (<1 mm to several centimetres). Typical sedimentary structures present include wave-ripple and combined-flow ripple lamination, and a small proportion of layers with normal grading, parallel lamination (both continuous and discontinuous), and starved-ripple cross-lamination	Low to moderate BI (1–4), low trace-fossil intensity. Ichnogenera present: navichnia, *Phycosiphon* and more common *Fugichnia* (escape structures) upsection
CMS	Middle shelf	Moderate to high	Common silt lamina to lamina-sets (thickness ranging from a few millimetres to several centimetres). Most primary sedimentary features are disrupted or absent due to pervasive bioturbation. Remnant preserved wave-ripple cross-laminations can be identified locally	Moderate to high BI (3–6) and trace-fossil diversity. Ichnogenera present: *Phycosiphon*, *Chondrites*, *Planolites*, C*ylindrichnus, Teichichnus, Schaubcylindrichnus freyi*, *Zoophycos* and *Thalassinoides*
SSM	Inner shelf to distal lower shoreface	High (maximum)	Most silt/sand lamina to lamina-sets in this facies are sharp-based and range from a few to several centimetres in thickness (a few sandstone beds can be as thick as 14 cm in outcrop). A wide range of sedimentary structures are present including common wave-ripple lamination, combined-flow ripple lamination, hummocky cross-stratification (HCS), a small amount of starved ripple and current ripple lamination, normal (and rare inverse) grading, and local soft sedimentary deformation	Highly variable BI (0–6) and trace-fossil diversity. Ichnogenera present: *Phycosiphon*, *Chondrites*, *Planolites*, *Schaubcylindrichnus freyi*, *Teichichnus*, *Thalassinoides, Skolithos and Ophiomorpha*

setting and relative changes of sea level (Williams *et al.*, 2001; Li *et al.*, 2015; Birgenheier *et al.*, 2017). In the laboratory, grain-size parameters (size and distribution) were further calibrated by semi-quantitatively comparing petrographic and scanning electron microscope (SEM) photomicrographs of selected samples at a range of magnifications.

A variety of sedimentary structures (such as abundance and continuity of laminae, grading, ripple forms, scours, etc.) and biogenic features (trace fossil types and bioturbation intensity) were documented. The Bioturbation Index (BI) of Taylor & Goldring (1993) was used to characterize the bioturbation intensity in these rocks, and the terminology of MacEachern *et al.* (2007) was used to identify specific burrow types. A facies key that summarizes the various aspects of sedimentary and biogenic features documented in this study is shown in Fig. 5.

The facies scheme used in this study is summarized in Table 1 and presented in greater detail in Li & Schieber (2018a). To characterize the variations in the rock composition and textural characteristics throughout the Tununk Shale, 41 polished thin sections (20 to 25 μm thick) and 48 ion-milled samples (up to 12 mm diameter) were prepared from samples representing all lithofacies and microfacies types throughout three measured sections. Detailed petrographic examination of polished thin sections and ion-milled samples were conducted using a petrographic microscope and an FEI Quanta 400 SEM (FEI Company, Hillsboro, OR, USA). The SEM was operated at 15 kV and a working distance of 10 mm. Energy-dispersive X-ray spectroscopy was used to determine the composition and mineralogy of individual grains.

For sequence stratigraphic analysis, this study focused on the basic characteristics of parasequences, system tracts and sequences, and endeavoured to employ objective criteria for their recognition. Parasequences are the fundamental building blocks of depositional sequences. They occur in all system tracts and are characterized by distinctive upward-shallowing successions of relatively conformable beds and bedsets bounded by surfaces of flooding, abandonment or reactivation and their correlative surfaces (Van Wagoner *et al.*, 1990; Catuneanu *et al.*, 2009; Abreu *et al.*, 2014). A parasequence set is a succession of genetically related parasequences forming a distinctive stacking pattern (for example, progradational, retrogradational and aggradational). Based on stratal stacking patterns, position within the sequence and types of bounding surfaces, different system tracts can be identified (Van Wagoner *et al.*, 1990); specifically lowstand, transgressive and highstand system tracts (LST, TST and HST) (Vail, 1987; Van Wagoner *et al.*, 1987). In addition a falling-stage system tract (FSST) has been identified in a number of studies (Hunt & Tucker, 1992; Posamentier *et al.*, 1992). Key stratal surfaces that divide sequences into different system tracts include the sequence boundary (SB), the transgressive surface (TS), and the maximum flooding surface (MFS; Van Wagoner *et al.*, 1990).

PARASEQUENCES, SYSTEM TRACTS AND KEY STRATIGRAPHIC SURFACES IN THE TUNUNK SHALE

Within each measured section, at least 49 parasequences can be identified in the Tununk Shale based on variations in average grain size, sedimentary facies, trace-fossil associations and bioturbation intensity. Parasequences range in thickness from 40 cm to 12 m, while the thickness of most (>80%) parasequences in the Tununk Shale ranges from 1 to 6 m. Based on parasequence stacking patterns (for example, progradational, aggradational and retrogradational), the 49 parasequences can be grouped into 11 system tracts, and four depositional sequences can be identified (Figs 4 and 6). Changes in parasequence stacking patterns are also reflected in the outcrops of the Tununk Shale, which are characterized by successive alternations between resistant ledges and non-resistant slopes (Fig. 7). The most resistant intervals in outcrops correspond to LSTs of sequences 2 to 4 and are laterally continuous between all three measured sections (Figs 4, 6 and 7). Because the lithofacies characteristics and stratal stacking patterns show little variability among all three measured sections (Fig. 6), only the stratigraphic section measured at Salt Wash is presented here in detail (Fig. 4). In the Tununk Shale in the present study area, the MFS of sequence 1 occurs slightly above the boundary between the SCM and the CSSM lithofacies. The surfaces that separate lithofacies CMS from lithofacies SCM and lithofacies SSM from lithofacies CMS correspond to the basal sequence boundaries of sequences 3 and 4, respectively (Figs 4 and 6).

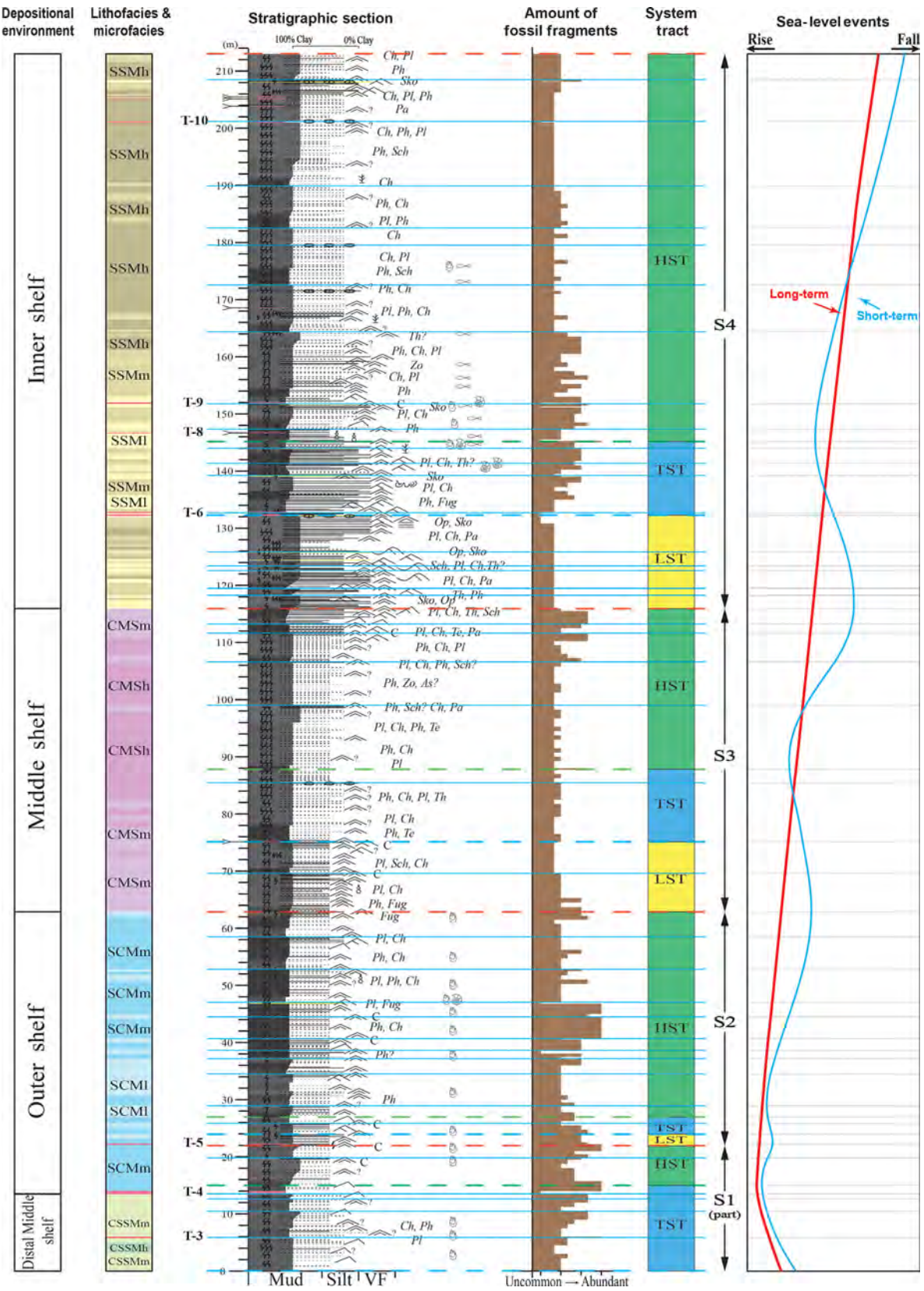

Fig. 4. The measured stratigraphic section at Salt Wash, with logs of relative amount of fossil fragments, lithofacies packages and microfacies, within a sequence stratigraphic framework. The same stacking pattern of lithofacies packages and facies characteristics are also observed in the measured sections at North Caineville and South Caineville. The sedimentology and depositional environments of the Tununk Shale are discussed in detail in Li & Schieber (2018a). The relative sea-level curves depict the second-order Greenhorn cycle, which has superimposed higher-order sea-level cycles. See Fig. 3 for the location of measured sections and Fig. 5 for facies key. LST, lowstand system tract, TST, transgressive system tract; HST, highstand system tract.

The following section will describe and summarize parasequence styles in the four depositional settings (inner to outer shelf) represented by the aforementioned lithofacies packages (Table 1). Focus is on the parasequence expression in the CSSM lithofacies using sequence 1 TST, in the SCM lithofacies using sequence 2 LST, in the CMS lithofacies using sequence 3 LST, and in the SSM lithofacies using sequence 4 LST. In addition, how parasequences in the TSTs and HSTs differ from those in the LSTs are described briefly and the overall stacking patterns in each sequence are discussed.

Sequence 1 (distal shelf to outer shelf environment)

In the study area, the Tununk Shale disconformably overlies non-marine and paralic deposits of the Dakota Sandstone. The base of the Tununk Shale is characterized by a conglomeratic layer containing pebbles of chert and fine-grained quartzite (Eaton *et al.*, 1990), overlain by a regionally extensive oyster coquina containing *Pycnodonte newberryi* (Stanton) (Fig. 8). The conglomeratic layer was interpreted as deposited during subaerial exposure of the study area in response to base-level fall (Eaton *et al.*, 1990). The oyster coquina represents a transgressive lag deposit that formed during the subsequent base-level rise when the conglomerate was reworked on a ravinement surface (Eaton *et al.*, 1990; Gardner & Cross, 1994). Bentonite beds T1 and T2 which are present in the laterally equivalent Topic Shale in southern Utah do not occur in the basal Tununk Shale of the Hanksville study area (Figs 2 and 4; Zelt, 1985; Leithold, 1994). The disconformity at the base of the Tununk Shale, therefore, represents a composite surface where a sequence boundary (SB) is combined with a transgressive surface (TS) of marine erosion.

Above the TS lies the TST of sequence 1 (S1), which consists of CSSM lithofacies deposited on the distal middle shelf (Fig. 4; Table 1). In this setting parasequences are characterized by a slight coarsening-upward trend that is recorded by upward increases in the silt/sand content and the abundance of silty/sandy laminae

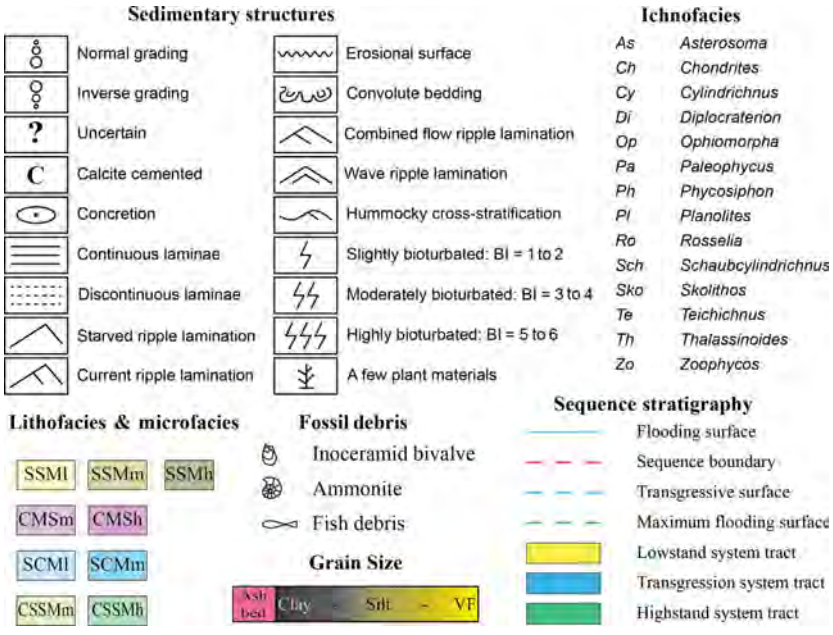

Fig. 5. Facies key for sedimentological and sequence stratigraphic analyses presented in this study. Four lithofacies packages were recognized in the Tununk Shale (Li & Schieber, 2018a,b), including: (i) carbonate-bearing, silty and sandy mudstone (CSSM); (ii) silt-bearing, calcareous mudstone (SCM); (iii) carbonate-bearing, silty mudstone to muddy siltstone (CMS); and (iv) non-calcareous, silty and sandy mudstone (SSM). The lower case letters 'l', 'm' and 'h' following each lithofacies name represent low, medium and high bioturbation intensity, respectively.

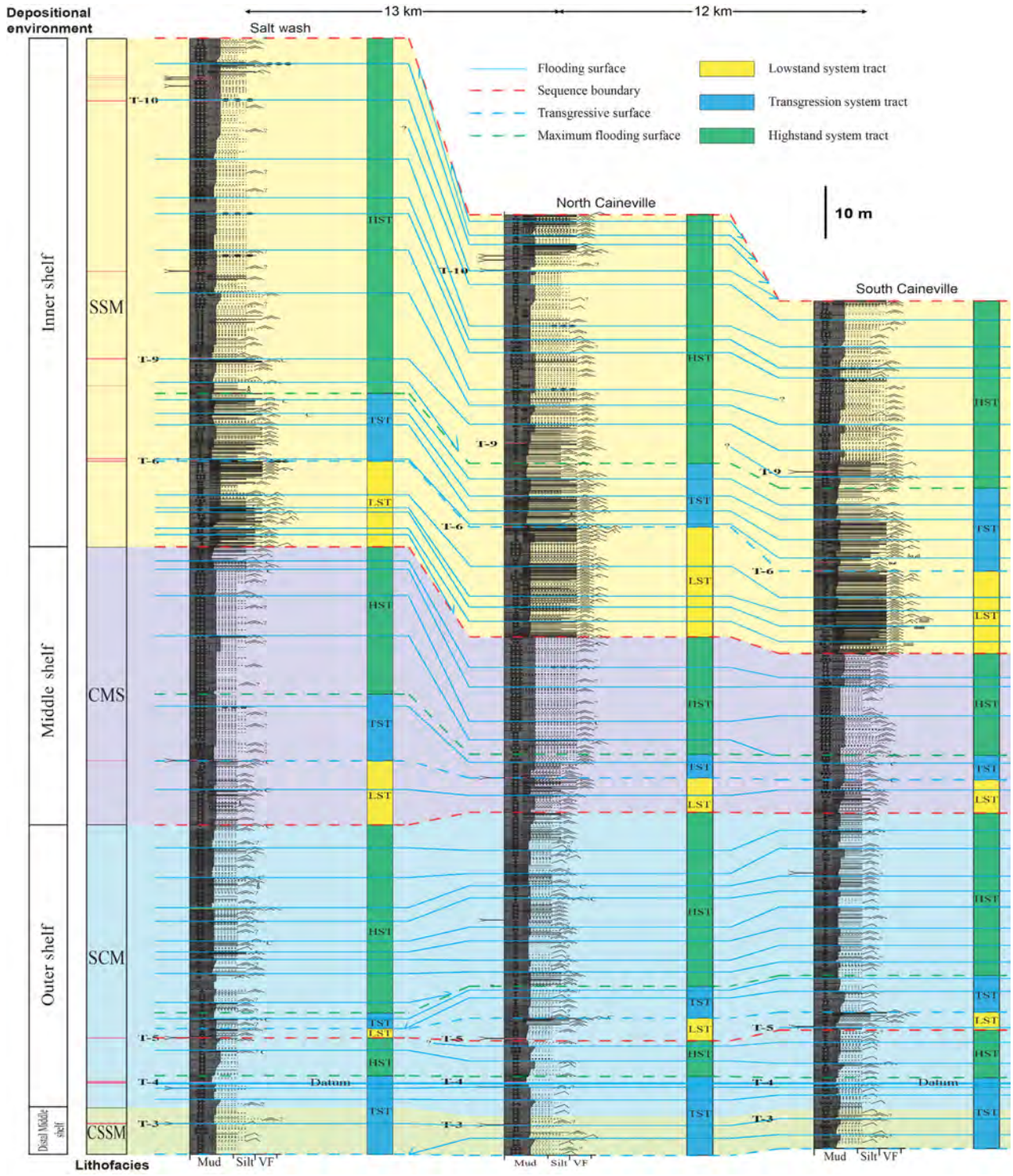

Fig. 6. North-east to south-west stratigraphy of the Tununk Shale in the study area. Three sequence boundaries are recognized in the Tununk Shale and four depositional sequences are defined. See Fig. 5 for facies keys.

(Fig. 9). Parasequence thickness ranges from around 0·7 to 5·9 m, with an average of 2·4 m (Fig. 10). Bioturbation intensity is moderate to high throughout a parasequence. Common trace fossil types include navichnia (sediment-swimmer traces), *Phycosiphon*, *Chondrites* and rare

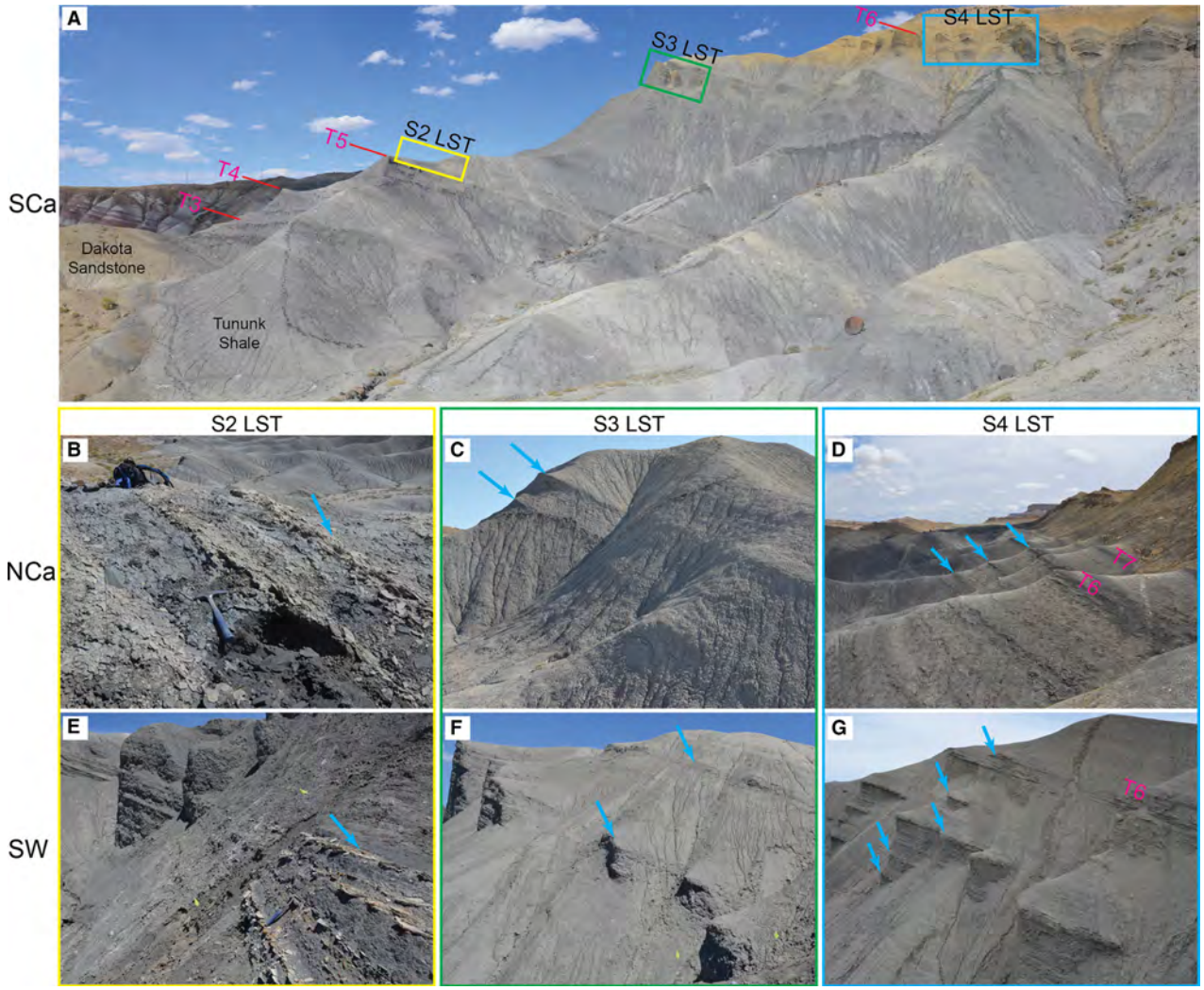

Fig. 7. The outcrops of the Tununk Shale are characterized by successive alterations of resistant ledges and non-resistant slopes, which are due to variations in average grain size and dominant lithology. The resistant ledges in outcrops that represent the lowstand system tracts (LSTs) of sequence 2, 3 and 4 (Fig. 5) are highlighted in yellow, green and blue boxes, respectively, and are laterally continuous in the study area. Each LST consists of one to multiple coarsening-upward parasequences. Parasequence boundaries (flooding surfaces) are indicated by blue arrows. See Fig. 3 for locations of measured sections and Fig. 6 for the thickness of LST parasequences of different sequences. SW: Salt Wash, NCa: North Caineville, SCa: South Caineville.

Planolites (Fig. 11A and B). Within this context, lower portions of parasequences are commonly characterized by discontinuous or disrupted silty/sandy laminae (Fig. 11A). Upward, distinctive sedimentary features including starved current ripple and starved wave ripple cross-laminations become more common (Fig. 11B).

Silt-sized to sand-sized particles in the CSSM lithofacies are dominated by detrital grains (for example, quartz and feldspar), with a minor amount of biogenic carbonate particles such as foraminifera tests (dominantly planktonic), faecal pellets (composed almost exclusively of coccolith debris) and shell fragments (principally inoceramid bivalve fragments) (Fig. 12A and B). The foraminifera tests are mostly filled with calcite spar and minor or trace amounts of pyrite and authigenic clays including kaolinite and smectite (Fig. 12B). Parasequence sets of the TST show a retrogradational stacking pattern characterized by thinner and finer parasequences upward (Figs 4 and 12). Over the course of the TST, the CSSM lithofacies grades upward into SCM lithofacies (Fig. 11C), and the

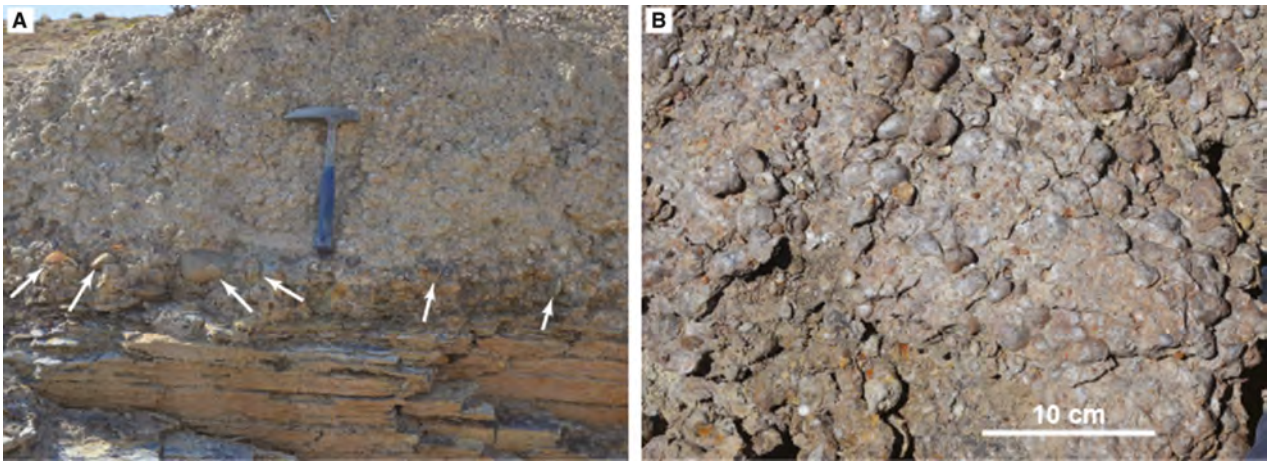

Fig. 8. Outcrop photographs showing the characteristics of the base of the Tununk Shale. (A) Above the shallow marine deposits of the Dakota Sandstone, the conglomeratic layer consists of pebbles (white arrows) and is overlain by regionally extensive oyster coquina containing *Pycnodonte newberryi* (Stanton). The hammer for scale is 33 cm in length. (B) Plan-view of the oyster coquina.

relative amount of silt-sized to sand-sized detrital particles gradually decreases as biogenic calcareous particles increase (Fig. 12D and E). The fine-grained matrix also becomes more calcareous upward due to increasing amounts of coccoliths (Fig. 12F). Whereas BI may remain moderate to high, trace-fossil diversity and burrow size gradually decrease upward towards the MFS (Fig. 11C).

Other than lithology, HST parasequences are similar to those of the TST (Fig. 9) in S1. The HST parasequences consist of the SCM lithofacies and range from 1 to 5 m in thickness (Fig. 10). The coarsening-upward trend of parasequences is expressed in the upward increase of the abundance and lateral continuity of wavy laminae, which are made dominantly of silt-sized to sand-sized calcareous particles such as foraminifera tests (dominantly planktonic), faecal pellets and shell fragments (Figs 9 and 11D). The BI remains moderate throughout a given parasequence but may decrease slightly towards the top of a parasequence when wavy laminae become more common (Fig. 9). The HST parasequences are characterized by overall low trace-fossil diversity, similar to the TST (Fig. 11C and D).

Sequence 2 (outer shelf environment)

Sequence 2 (S2) consists of the SCM lithofacies deposited in the outer shelf environment (Fig. 4; Table 1). The basal SB of S2 is capped by a thin (a few millimetres or less) lag layer of broken inoceramid fragments at the base of a *ca* 5 cm wave-rippled bed. Above the SB, the LST in S2 consists of one parasequence, which shows an abrupt increase in the abundance of resistant layers in outcrops (Figs 6 and 7). The thickness of the LST parasequence ranges from 50 cm to 4·3 m, with an average of 2·4 m among three measured sections. Compared to the underlying HST of S1, LST parasequences in S2 show more common and distinct (thicker and more laterally continuous) storm-generated sedimentary structures such as parallel to slightly wavy laminae, wave ripple and combined-flow ripple laminations (Fig. 13). In the LST, the lower part of a given parasequence shows common bioturbation and few distinct sedimentary features (Fig. 14A), whereas the upper part shows an increasing amount of thicker (up to several centimetres) wave ripple and combined-flow ripple laminations and lower BI (Fig. 14B to D). Trace-fossil diversity remains low in the S2 LST.

In the lower part of a typical LST parasequence, silt-sized to sand-sized carbonate particles such as faecal pellets, foraminifera tests and shell fragments are commonly scattered in the fine-grained calcareous matrix (rich in coccolith debris; Fig. 15A). Towards the top of a given LST parasequence, these silt-sized to sand-sized carbonate particles are more prone to be concentrated along wavy laminae and show preferred orientation (Figs 14B to D and 15B to F). Wave ripple and combined-flow ripple laminations

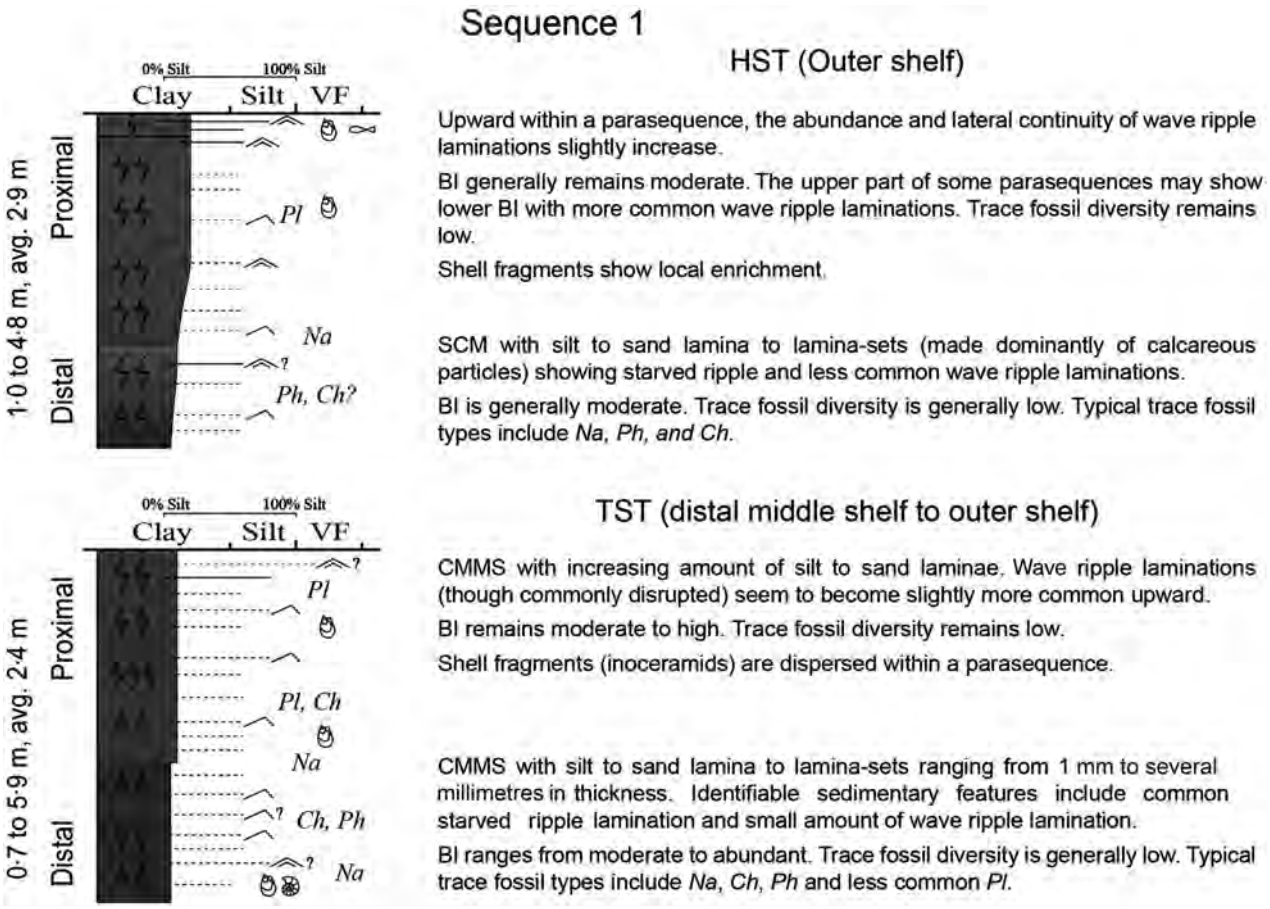

Fig. 9. Schematic drawings of parasequence styles in sequence 1. See Fig. 5 for facies key.

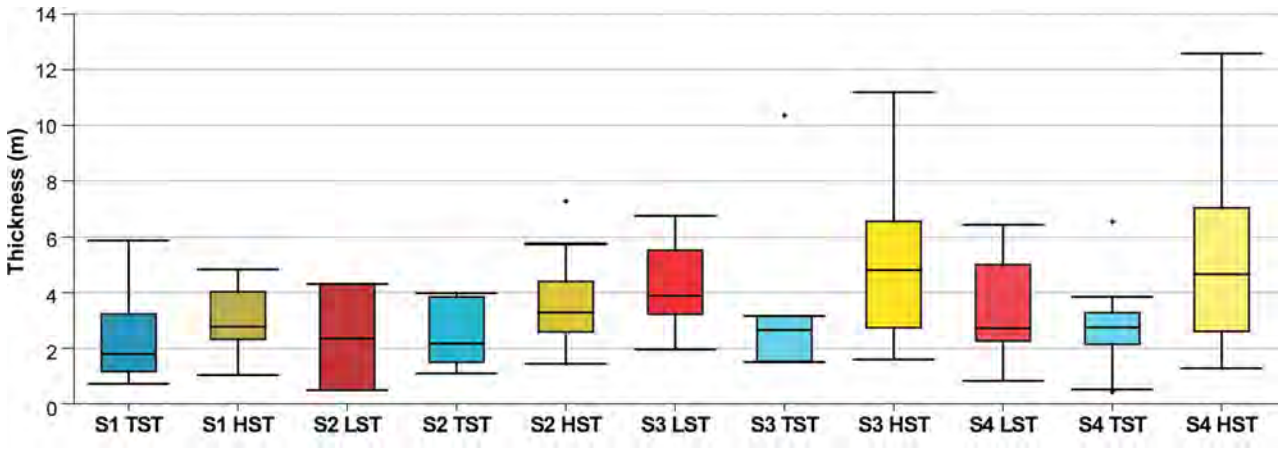

Fig. 10. Box plot showing the distribution of parasequence thickness in different system tracts of the Tununk Shale. Data of parasequence thickness were compiled from all three measured sections. Note that outliers with excessive thickness tend to occur in S2 HST, S3 TST, and S4 TST. It is possible that each of these thick parasequences (outliers) actually consists of more than one thinner parasequences. Because TST and HST deposits are usually more fine-grained and more susceptible to weathering (non-resistant slopes in Fig. 7), thin parasequences are not as readily resolved. Therefore, the total number of parasequences documented in each measured section may underestimate the actual number of parasequences in the Tununk Shale. LST, lowstand system tract, TST, transgressive system tract; HST, highstand system tract.

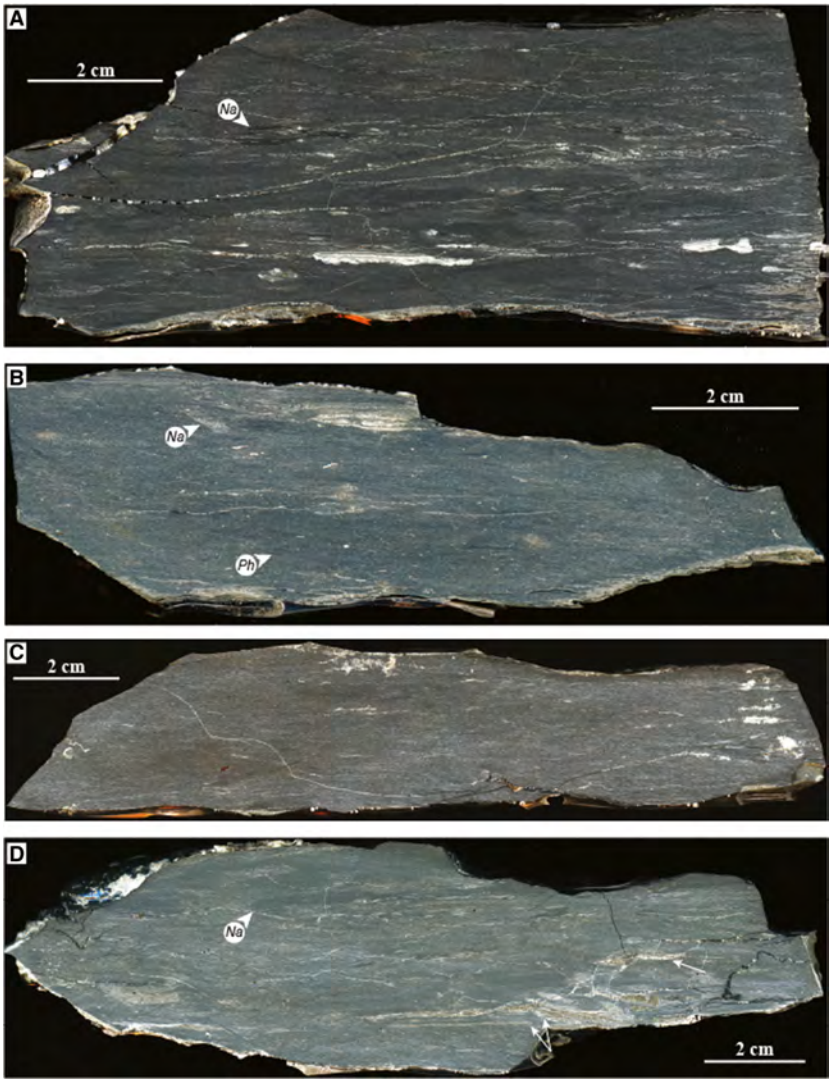

Fig. 11. Scanned and processed images of polished slabs made from samples in S1. (A) CSSMm facies from the lower interval of a transgressive system tract (TST) parasequence showing discontinuous silt/sand laminae and lamina-sets with scoured bases and common fabric disruption by sediment-swimmers (*Na: navichnia*). (B) CSSMm facies from the upper portion of a TST parasequence that becomes siltier and shows laterally discontinuous sandy wave-ripple laminations (*Ph: Phycosiphon*). (C) Close to the maximum flooding surface in S1, the SCMm facies shows mottled texture mostly due to navichnia (sediment-swimmer traces) and rare preserved sedimentary features. (D) SCMm facies from the highstand system tract in S1. Above the MFS, wavy laminae consisting dominantly of biogenic carbonate particles including foraminifera tests and fossil fragments (dominantly inoceramid bivalve fragments, which are indicated by white arrows) gradual increase in abundance. Sedimentary features are commonly disrupted due to bioturbation. Typical trace-fossil types include *Na* and *Ph*.

made dominantly of foraminifera tests tend to be better cemented by early diagenetic calcite close to the top of a parasequence, forming resistant layers in outcrops (Fig. 15E and F).

The TST parasequences of S2 are characterized by an abrupt decrease in the abundance of calcareous and silty laminae and an increase in BI (Figs 13 and 14E). Parasequences of the early HST of S2 are similar to those in the HST of sequence 1. Towards late HST in S2, parasequences show a gradual increase in the abundance and thickness of wave ripple laminations, trace-fossil diversity and burrow size up-section (Figs 13 and 14F).

Sequence 3 (middle shelf environment)

The SCM lithofacies abruptly changes into the CMS lithofacies across the SB at the base of sequence 3 (S3). The LST in S3 consists of three parasequences, and range from 2·0 to 6·7 m in thickness, with an average of 4·2 m (Fig. 10). Compared to S2, parasequences in the LST of S3 are characterized by moderate to high BI and a distinctly higher trace-fossil diversity (Figs 16 and 17). Common types of trace fossils in this facies are those produced by deposit-feeding organisms such as *Phycosiphon*, *Chondrites*, *Planolites*, *Schaubcylindrichnus freyi*, *Cylindrichnus*, *Zoophycos* and *Thalassinoides* (Fig. 17). The CMS lithofacies is characterized by significantly higher amounts of detrital silt particles and clays, and a subordinate amount of carbonate particles of biogenic origin (Fig. 18A to C). Although primary sedimentary features are commonly disrupted, remnant wave ripple laminations made dominantly of silt-sized detrital grains become thicker and more common upward within the LST parasequences (Figs. 17A, 17B and 18A to C).

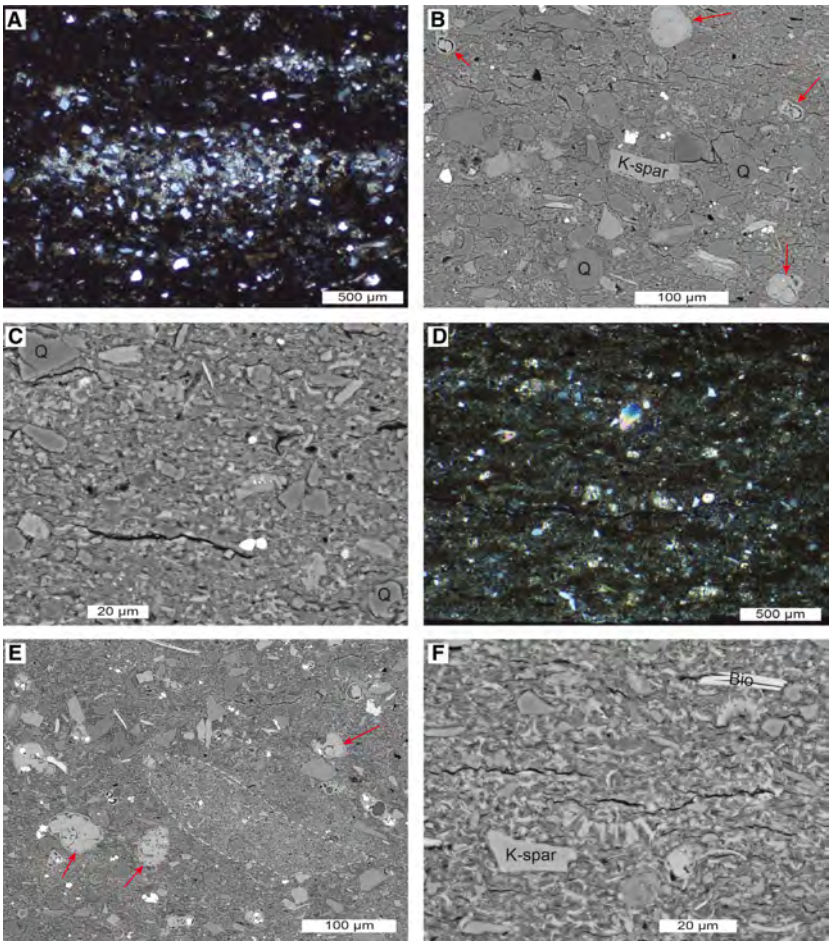

Fig. 12. (A) Photomicrograph (cross-polarized light: CPL) showing a starved ripple lamina in the CSSMm facies in the transgressive system tract (TST) of S1. The lamina is made dominantly of silt-sized to sand-sized detrital grains (quartz and feldspar showing low interference colour) and a minor amount of biogenic carbonate particles (high interference colour). (B) Photomicrograph showing a representative view from the same sample of (A). Silt-sized to sand-sized particles include a dominant amount of quartz and feldspar and a minor amount of foraminifera tests (indicated by red arrows). The foraminifera tests are mostly filled with calcite spar and minor or trace amounts of pyrite and authigenic clays including kaolinite and smectite. (C) Photomicrograph showing a representative view of the fine-grained matrix in the CSSMm facies in the TST of S1. The fine-grained matrix is dominated by fine-grained detrital silt (mostly quartz) and clays and a small amount of coccolith debris. (D) Photomicrograph (CPL) showing the mottled texture in the SCMm facies close to the maximum flooding surface (MFS) in S1. Silt-sized to sand-sized particles in this facies consist of a major proportion of carbonate particles (particles showing high interference colour). The fine-grained matrix consists dominantly of coccolith debris [thus showing brighter interference colour compared to (A)]. (E) The SCMm facies close to the MFS in S1 consists of a dominant amount of biogenic carbonate particles including foraminifera tests filled with calcite (red arrows) and faecal pellets (white dashed lines). The average grain size of detrital particles (darker grey) is distinctly finer compared to (B). (F) A representative view of the fine-grained matrix in the SCMm facies close to the MFS in S1. Note the abundant coccolith debris. Q, quartz; K-spar, potassium feldspar; Bio, biotite. (B), (C), (E) and (F) were taken in backscatter electron mode.

Parasequences in the TST of S3 show moderate bioturbation to complete homogenization and much fewer remnant wave ripple laminations (Figs 16 and 17C). The MFS in S3 is characterized by a carbonate concretionary layer containing abundant broken fossil fragments and phosphatic particles (Fig. 17D). Above the MFS, bioturbation intensity remains moderate to high (BI = 3 to 6) in the HST (Fig. 16). Trace-fossil diversity, as well as the abundance of storm-generated sedimentary structures, gradually increases upward during

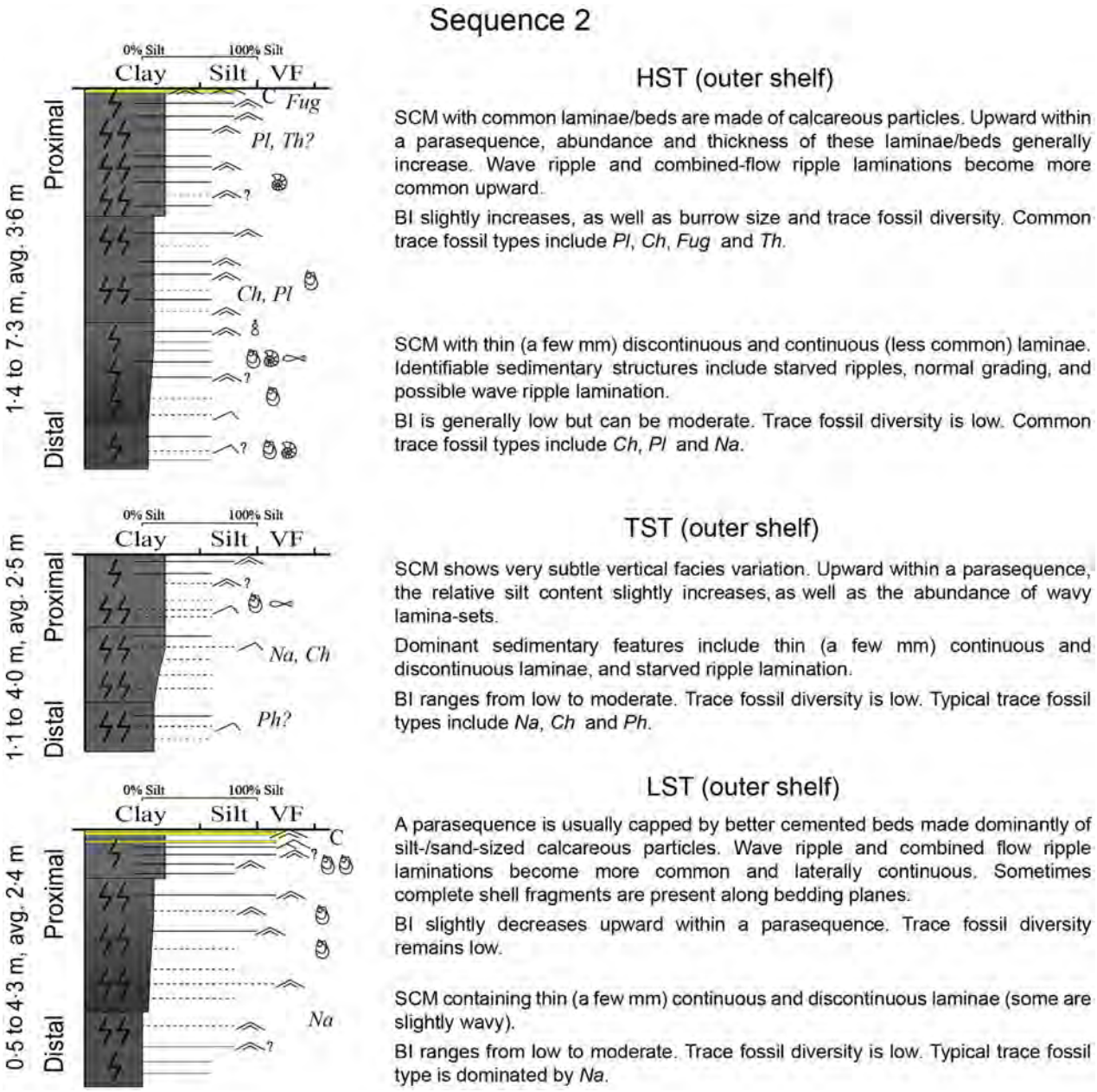

Fig. 13. Schematic drawings of parasequence styles in sequence 2. See Fig. 5 for facies key and Fig. 10 for ranges of parasequence thickness in different system tracts.

the HST (Fig. 17E). Due to common bioturbation, the coarsening-upward trend of parasequences is not always easy to recognize in outcrop, especially in the TST and HST. Although the relative proportion of carbonate particles derived from primary productivity is low overall, certain horizons in S3 are characterized by abrupt increases in carbonate content. These layers are typically better cemented by early diagenetic calcite and can also be associated with carbonate concretion layers, or concentration of fossil fragments (Figs 16, 17D and 18D to F). All of these features tend to occur in the intervals below flooding surfaces.

Sequence 4 (inner shelf environment)

The basal SB of sequence 4 (S4) shows minor erosional features (erosional base of a

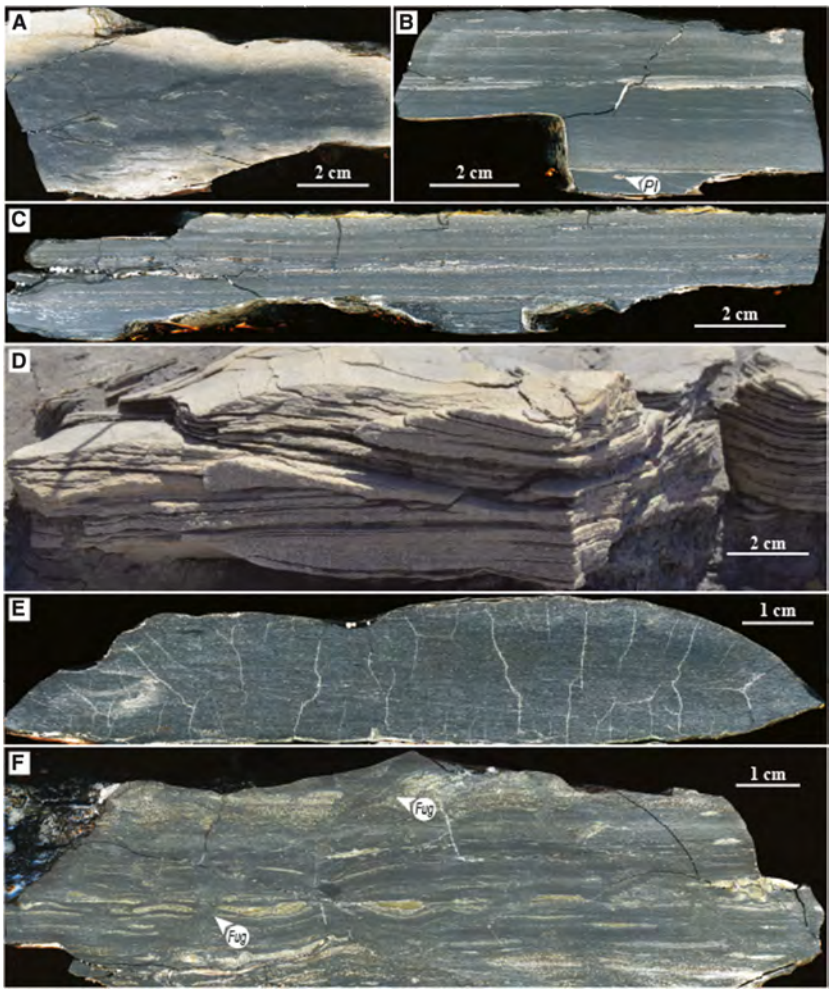

Fig. 14. Scanned and processed images of polished slabs and outcrop photographs from S2. (A) SCMm facies from the lower interval of the LST parasequence showing sediment-swimmer traces. (B) and (C) SCMl facies from the upper interval of the LST parasequence. Parallel to slightly wavy laminae consist dominantly of silt-sized to sand-sized carbonate particles including planktonic foraminifera tests, faecal pellets and shell fragments. BI ranges from 0 to 1. *Pl: Planolites*. (D) The bed capping the LST parasequence shows wave ripple and combined-flow ripple laminations. Laminae consist dominantly of silt-sized/sand-sized carbonate particles. (E) SCMm facies from the TST (close to the MFS) showing mottled texture with rare preserved sedimentary features. (F) SCMm facies from a parasequence in the late HST that shows wavy laminae. These laminae consist dominantly of carbonate particles with increasing amounts of detrital silt particles. Burrow size gradually increases in the HST. *Fug: Fugichnia* (trace-fossil escape structure).

centimetre-scale wave-rippled bed) and separates the CMS lithofacies from the overlying SSM lithofacies. The LST in S4 consists of five or six parasequences. The thickness of parasequences in the LST ranges from 0·8 to 6·4 m, with an average of 3·1 m (Fig. 10). Parasequences in the LST of S4 contain a distinctly high proportion of detrital siltstone and sandstone beds, as well as a wide variety of storm-generated sedimentary structures (Fig. 19). A typical LST parasequence can be divided into three intervals (Fig. 19). The lower part is characterized by slightly bioturbated mudstones with thin (millimetres to a few centimetres) siltstone/sandstone beds (Fig. 20A). The middle part of a parasequence is characterized by moderately bioturbated sandy mudstones, with disrupted but still recognizable storm-generated sedimentary structures (Fig. 20B). The uppermost part of a parasequence shows low BI, and more common and thicker sandstone beds containing wave ripple laminations or hummocky cross-stratification (HCS) (Fig. 20C and D). Although these three intervals may not be present in every given parasequence, a general coarsening-upward trend can always be observed. Upward in a parasequence, the dominant trace-fossil types usually change from dominant deposit-feeding traces (for example, *Phycosiphon*, *Chondrites*, *Planolites*, *Schaubcylindrichnus freyi*, *Teichichnus,* etc.) to more common suspension-feeding traces (for example, *Skolithos* and *Ophiomorpha*) (Fig. 19). In S4, the SSM lithofacies contains almost exclusively siliciclastic particles derived from terrigenous sources and only a small amount of reworked fossil fragments (Fig. 21).

The TS capping the LST in S4 is characterized by a carbonate concretion layer (Fig. 20E). Parasequences in the overlying TST become thinner and finer (less silt and sand content) upward. Although storm-generated sedimentary structures such as silty/sandy wave ripple and

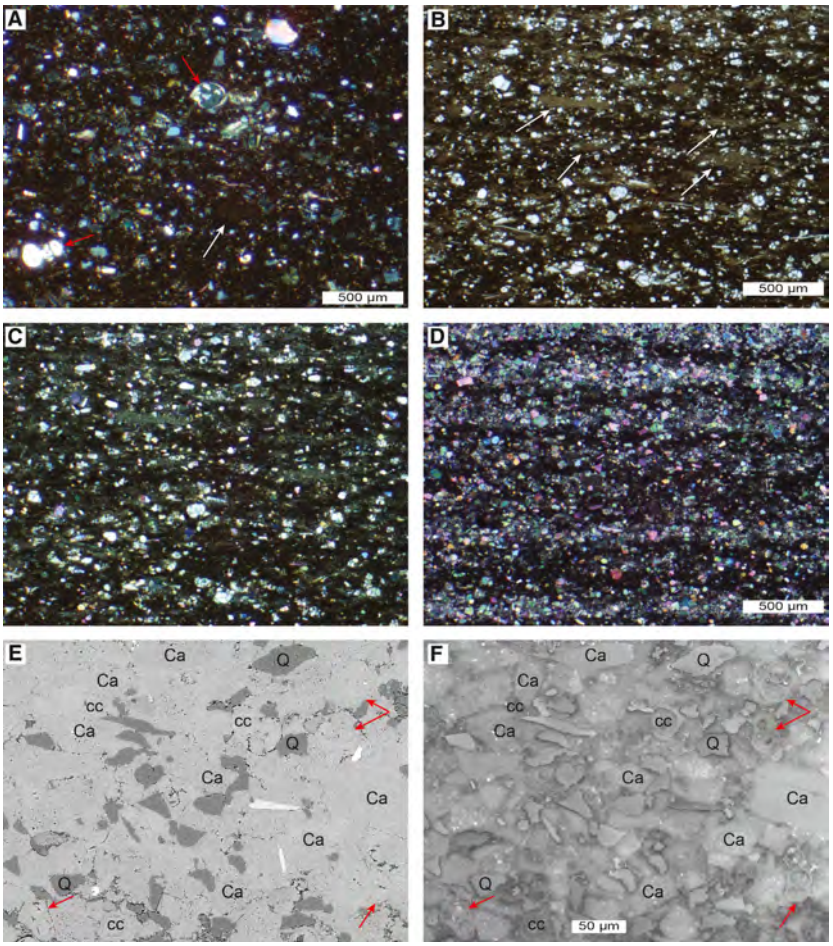

Fig. 15. Petrographic characteristics of the LST parasequence in S2. (A) Photomicrograph (CPL) showing the bioturbated texture of the SCMm facies in the lower interval of the LST parasequence. Carbonate particles including foraminifera tests (red arrows), faecal pellets (white arrow) and shell fragments (high interference colour) dominate over detrital grains. The foraminifera tests are mostly filled with calcite spar. (B) and (C) Photomicrographs (PPL: plane-polarized light and CPL) showing SCMl facies from the upper interval of the LST parasequence (darker intervals in Fig. 14B and C). Note that sand-sized faecal pellets (white arrows) and foraminifera tests are concentrated along laminae and show preferred orientation. (D) Photomicrograph (CPL) showing a representative view of the wave ripple lamination close to the top of the LST parasequence. The lighter and darker layers consist dominantly of silt-sized/sand-sized foraminifera tests (filled with calcite spar) and faecal pellets, respectively. (E) and (F) Photomicrographs (backscatter and secondary electron mode) showing a representative view of the wave ripple lamination close to the top of the LST parasequence. The lamina is made dominantly of silt-sized to sand-sized foraminifera tests (red arrows), carbonate shell fragments (Ca), a minor amount of detrital grains (mostly quartz), and pervasive calcite cement (cc). The concentration of these carbonate particles along wavy laminae indicates that they were reworked by storm-induced bottom currents. Q, quartz.

combined-flow ripple cross-laminations may still be common in a given parasequence, their thicknesses distinctly decreases upward in the TST (Fig. 19). Locally, soft sedimentary deformation features are observed in the TST (Fig. 20F). Compared to the LST, bioturbation intensity and diversity slightly decrease, whereas the relative amount of fossil fragments increases in the TST (Figs 4 and 19). The MFS in S4 is characterized by a very fine-grained sandstone bed showing planar and wave ripple laminations and enrichment of phosphatic particles, fish debris and bone fragments (Fig. 20G). Above the MFS, parasequences in the HST are characterized by moderate to high BI and common remnants of silty/sandy laminae (Fig. 20H). Remnant wave ripple and combined-flow ripple cross-laminations are more likely to be

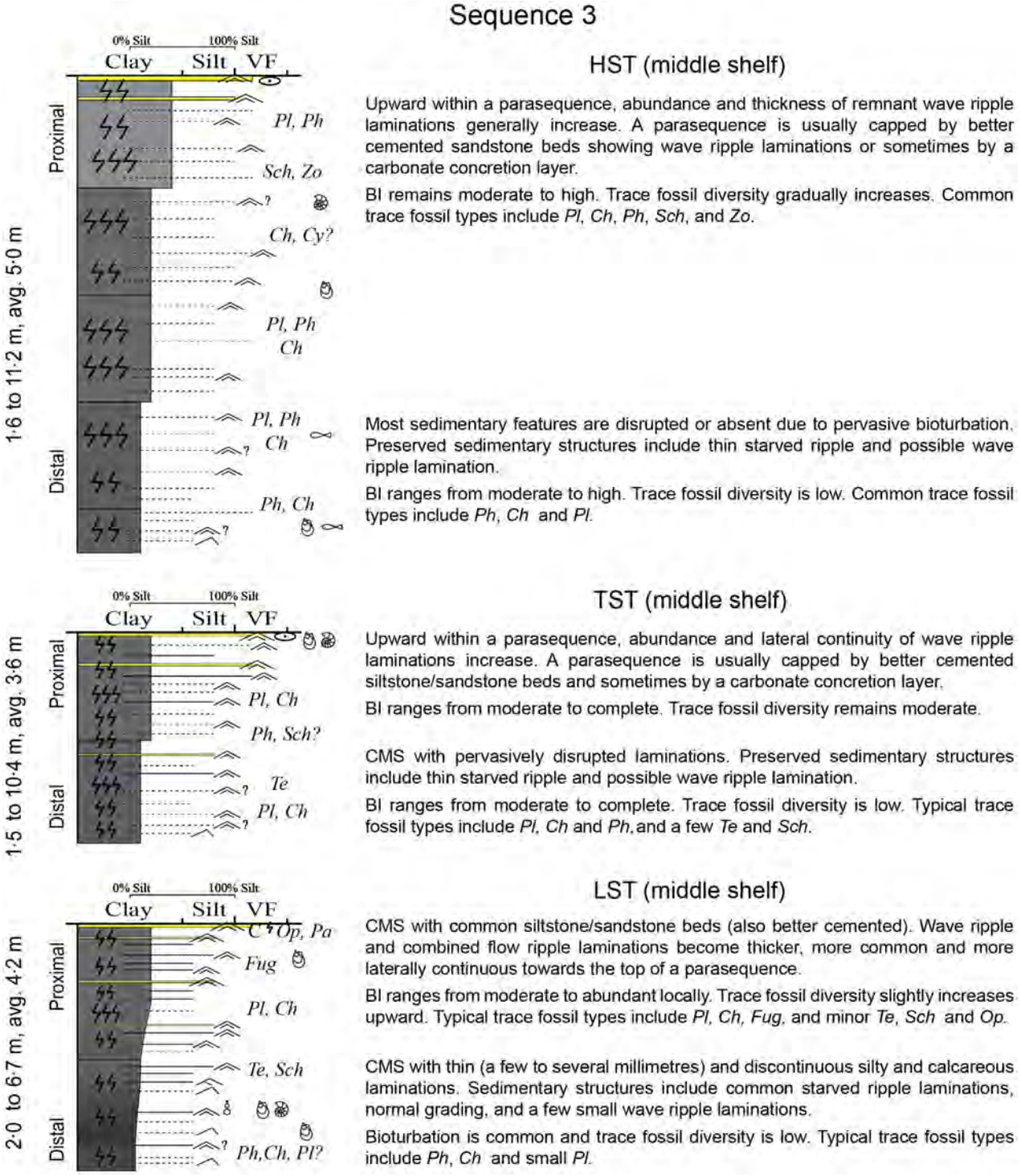

Fig. 16. Schematic drawings of parasequence styles in sequence 3. See Fig. 5 for facies key and Fig. 10 for ranges of parasequence thickness in different system tracts.

preserved towards the top of a parasequence (Fig. 19). In some parasequences, carbonate concretions are present below, or are immediately overlain by, the flooding surfaces (Fig. 19). Towards the late HST, remnant sandy wave ripple cross-lamination, as well as terrestrial organic matter become more common in parasequences up-section (Fig. 4).

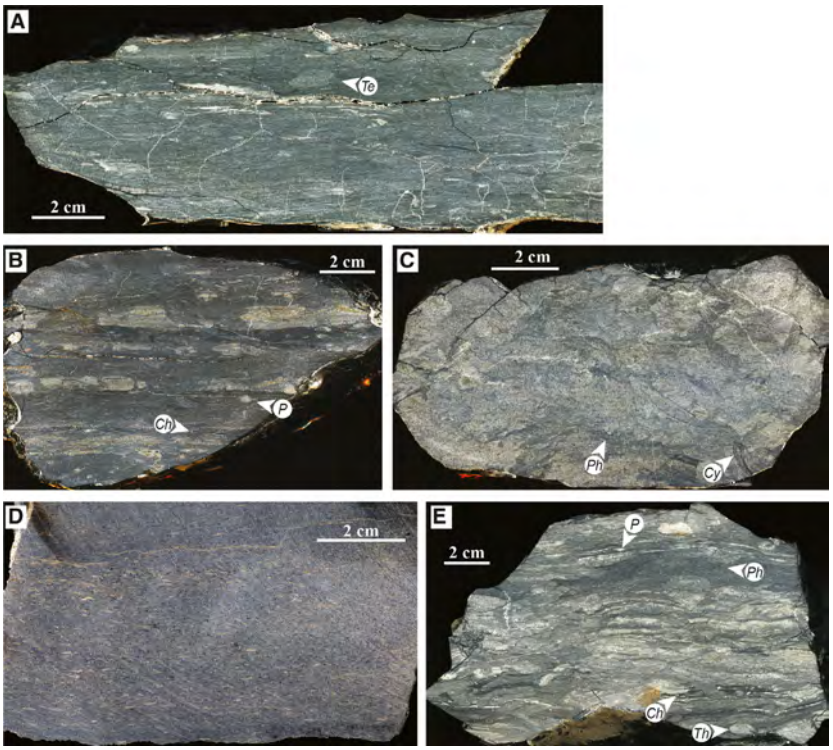

Fig. 17. Scanned and processed images of polished slabs from S3. (A) CMSm facies from the lower interval of a lowstand system tract (LST) parasequence that shows bioturbation and a few distinct laminae. *Te: Teichichnus*. (B) CMSm facies from the upper interval of a LST parasequence. Although commonly bioturbated, the preserved remnants of sedimentary structures (probably wave ripple laminae) become more common towards the top of the parasequence. The trace-fossil diversity also slightly increases upward. *P: Planolites*, *Ch: Chondrites*. (C) CMSh facies from a TST parasequence (close to the MFS). The pervasive bioturbation largely destroyed primary sedimentary structures. *Ph: Phycosiphon*, *Cy: Cylindrichnus*. (D) The MFS of S3 is characterized by a carbonate concretion layer containing abundant broken shell fragments. (E) CMSm facies from a parasequence in the late highstand system tract (HST). The preserved remnants of wave ripple laminae gradually become more common upwards in the HST. The relative amount of carbonate particles gradually decreases upward in the HST. *Th: Thalassinoides*.

DISCUSSION

Parasequence styles in the Tununk Shale

Parasequences formed in different depositional environments of the Tununk Shale show considerable variability in terms of lithofacies, sedimentary facies and bioturbation characteristics. During the initial Greenhorn transgression, sediment supply to the Tununk Shale was still dominated by siliciclastic components from the terrigenous input and had a minor amount of biogenic carbonate particles (Fig. 12A to C). In the distal middle shelf environment (S1 TST), coarsening-upward parasequences are characterized by upward increases in the amount of silt-sized/sand-sized detrital grains and sedimentary structures generated by bottom currents (for example, starved ripple and wave ripple laminations) (Figs 9, 11A and 11B). The moderate to high bioturbation index (BI) and low trace-fossil diversity indicate an overall slow sedimentation rate and some degree of environmental stress, mainly associated with the increasing water depth during the Greenhorn transgression.

Above the maximum transgression of the Greenhorn cycle, parasequences formed in the outer shelf environment (S1 HST to S2 HST) consist dominantly of carbonate particles derived from primary productivity and a minor amount of siliciclastic particles from terrigenous input (Fig. 15A to D). The coarsening-upward trend of parasequences in this environment is again reflected by an upward increase in the abundance of wave ripple or combined-flow

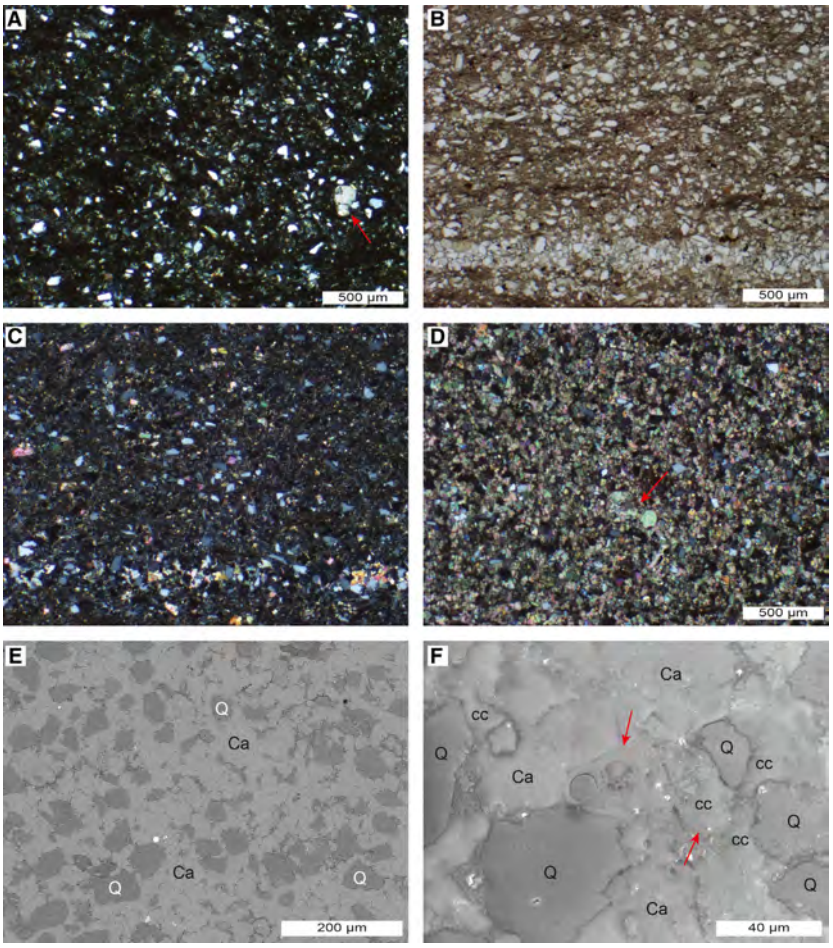

Fig. 18. Petrographic characteristics of S3. (A) Photomicrograph (CPL) showing the bioturbated texture in the CMSm facies from the lower interval of a parasequence in the LST. The relative amount of biogenic carbonate particles (for example, foraminifera tests, faecal pellets and coccolith debris) significantly decreases in S3, indicating an increasing degree of clastic dilution. (B) and (C) Photomicrographs (PPL and CPL) showing a remnant lamina (base of the image) in the CMSm facies from the upper interval of a parasequence in the LST. Note that detrital grains (quartz and feldspar showing low interference colour) dominate and that carbonate particles (high interference colour) only constitute a minor fraction. (D) Photomicrograph (CPL) showing a representative area in a calcite-cemented (note high interference colour) layer that caps a parasequence in the TST. (E) and (F) Photomicrographs (backscatter and secondary electron mode) showing the composition and texture of the same sample as (D). Detrital particles (mostly quartz), carbonate fragments (Ca, shell fragments) and a small amount of foraminifera tests are cemented by early diagenetic calcite (cc). Foraminifera tests are indicated by red arrows. Q, quartz.

ripple laminations, which nonetheless consist mostly of silt-sized/sand-sized carbonate particles such as foraminiferal tests, faecal pellets and shell fragments (Figs 13 to 15). Although being originally settled to the sea bottom from the upper water column, these silt-sized/sand-sized carbonate particles are hydrologically equivalent to quartz silt grains (Nowell *et al.*, 1981; Minoura & Osaka, 1992; Oehmig, 1993). The concentration of these carbonate particles along wavy laminae and wave ripple cross-lamination, as well as lower BI, towards the top of a given parasequence indicate that they were subject to more frequent reworking by storm-induced bottom currents owing to the shallowing of water depth (MacEachern *et al.*, 2005). Comparable observations have also been made in the Cretaceous Eagle Ford Shale of south-western Texas, USA (Schieber *et al.*, 2016), and in the Turonian sediments from Tanzania (Wendler *et al.*, 2016). Trace-fossil diversity in this environment remained low, mainly related to relatively high sea level and oxygen/food limitation during the second-order Greenhorn highstand (Savrda & Bottjer, 1991; Li & Schieber, 2018a).

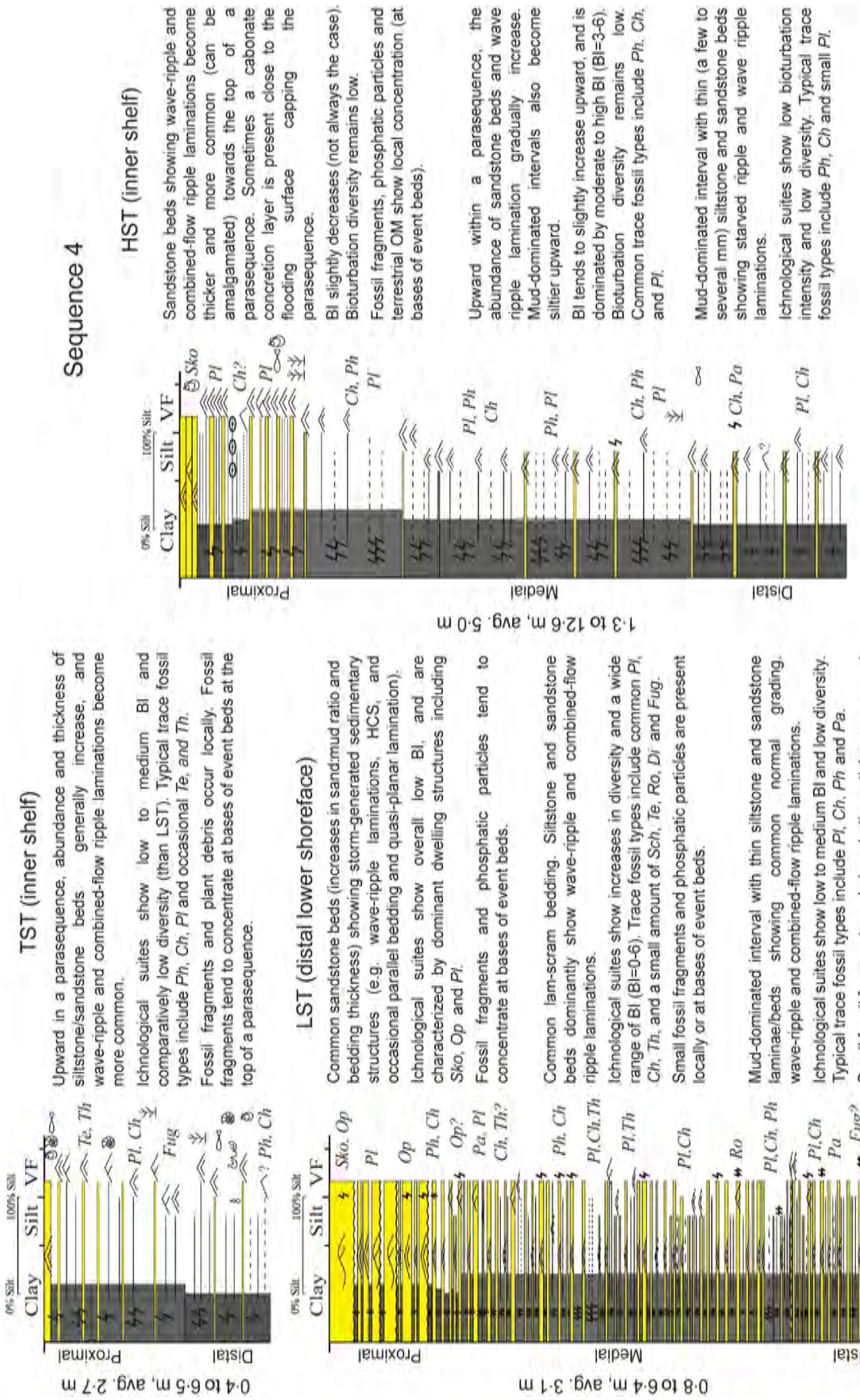

Fig. 19. Schematic drawings of parasequence styles in sequence 4. See Fig. 5 for facies key and Fig. 10 for ranges of parasequence thickness in different system tracts.

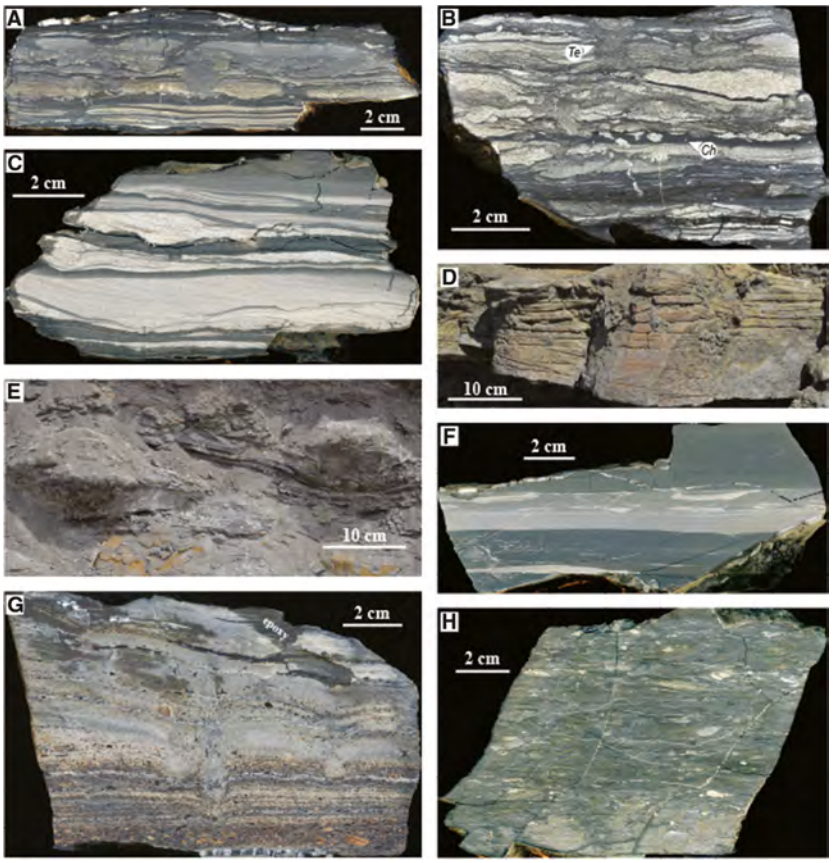

Fig. 20. Scanned and processed images of polished slabs and outcrop photographs from S4. (A) SSMm facies from the lower interval of a parasequence in the LST that shows thin disrupted silty wave ripple laminae. (B) SSMm facies from the middle part of a parasequence in the LST showing more common and thicker sandy wave ripple laminae. *Te: Teichichnus*, *Ch: Chondrites*. (C) SSMl facies from the upper portion of a parasequence in the LST showing rare bioturbation and common wave ripple and combined-flow ripple laminae with erosional bases. (D) A thick, very fine-grained sandstone bed that caps a parasequence in the LST and shows HCS. (E) The transgressive surface capping the LST is characterized by a carbonate concretion layer. (F) SSML facies from a parasequence in the TST that shows soft sedimentary deformation (load structures). (G) The MFS is marked by a sandstone bed that shows parallel to wavy laminae and a concentration of phosphatic particles and fossil fragments. (H) SSMh facies from a parasequence in the HST. Due to pervasive bioturbation, remnants of sedimentary features are difficult to identify. LST, lowstand system tract, TST, transgressive system tract; HST, highstand system tract.

During the regressive phase of the second-order Greenhorn cycle, parasequences formed in the middle shelf environment (S3) consist dominantly of detrital silt grains and a minor amount of carbonate particles derived from primary productivity (Fig. 18A to C). The moderate to high BI, as well as increases in BI and burrow size in the CMS lithofacies indicate more favourable substrate conditions related to shallowing water depth. Due to pervasive bioturbation, the coarsening-upward trends of parasequences in this setting are more difficult to identify. However, the preserved remnants of wave ripple laminae become more common towards the top of a given parasequence, consistent with a slight increase in sedimentation rate (Fig. 16).

During continued regression of the second-order Greenhorn cycle, parasequences formed in the inner shelf environment (S4) consist almost exclusively of siliciclastic grains of terrigenous origin (Fig. 21A to D). Due to comparatively shallow water depth in the inner-shelf environment, the coarsening-upward trends of parasequences are well marked by upward increases in thickness and abundance of silty and sandy beds with storm-generated sedimentary structures (for example, wave ripple and combined-flow ripple cross-lamination, HCS) (Fig. 19). No

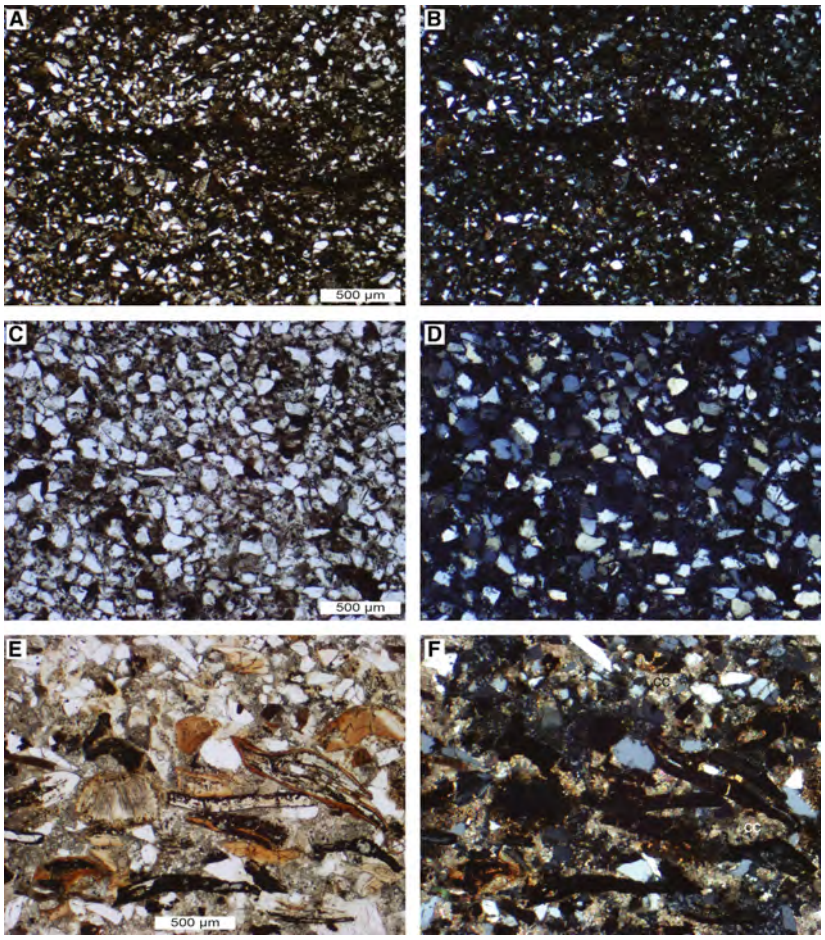

Fig. 21. Petrographic characteristics of S4. (A) and (B) Photomicrographs (PPL and CPL) showing the bioturbated texture in the SSMm facies from the lower interval of a parasequence in the lowstand system tract (LST). Carbonate particles in S4 are rare except for some fossil fragments. (C) and (D) Photomicrographs (PPL and CPL) that show an area within wave ripple laminae of the SSMl facies from the upper part of a parasequence in the LST. This bed consists almost exclusively of detrital grains (for example, quartz and feldspar). (E) and (F) The MFS of S4 is characterized by a sandstone bed that shows a concentration of fossil fragments (for example, fish debris and bone fragments) and phosphatic particles and is cemented by calcite (cc) (PPL and CPL).

simple trend can be summarized to describe changes in bioturbation intensity or diversity within these parasequences. To illustrate this complexity, lowstand system tract (LST) or highstand system tract (HST) parasequences in S4 could be taken as examples. These parasequences can be subdivided into three intervals (Fig. 19). The relatively low bioturbation intensity and diversity in the lower part of a given parasequence may be due to increased water depth after flooding, resulting in diminished oxygen supply or reduced nutrient/food availability (Savrda & Bottjer, 1991). Increases in BI, trace-fossil diversity and burrow size in the middle part can be interpreted to reflect improving bottom water oxygenation as water depth decreases, and frequency and magnitude of erosive depositional events are still low. The upper part of a given parasequence usually shows low BI, probably a reflection of increased sedimentation rate and more frequent and stronger storm events (Bentley & Nittrouer, 2003; Wheatcroft & Drake, 2003; MacEachern *et al.*, 2005). Similarly, parasequences developed in relatively proximal settings in the Mowry Shale, USA (latest Albian to earliest Cenomanian) can also be divided into three distinct intervals based on comparable trends in both sedimentary facies and bioturbation characteristics (Bohacs *et al.*, 2005). In proximal areas, the complex changes in bioturbation intensity and diversity within parasequences indicate that bioturbation is controlled by multiple factors such as oxygen and food supply, substrate type, sedimentation rate, etc. (Savrda & Bottjer, 1991; Bohacs *et al.*, 2005; MacEachern *et al.*, 2005). Notwithstanding these complexities, abrupt changes in BI or dominant trace-fossil types commonly occur across parasequence boundaries.

In all depositional sequences recognized in the Tununk Shale in this study, LST parasequences are marked by comparatively high abundance of distinct (relatively thick and laterally continuous) storm-generated sedimentary features (regardless of dominant mineralogy) and comparably low BI. The TST parasequences are characterized by overall common bioturbation, a minimal amount of remnant sedimentary features

and the lowest trace-fossil diversity. Bioturbation is also common in HST parasequences, but trace-fossil diversity, as well as the abundance of preserved remnants of storm-generated features gradually increases upward during the HST. In each sequence, TST parasequences have the smallest average thickness (Fig. 10), consistent with minimal sedimentation rate due to a longer transport pathway from the palaeoshoreline as a result of rising sea level. The average thickness of LST parasequences is smaller than that of HST parasequences in each sequence (Fig. 10). Based on sedimentary facies and bioturbation characteristics in LSTs and HSTs, this probably reflects more common reworking and erosion because of shallower water depth.

Identification of key sequence stratigraphic surfaces in the Tununk Shale

In this study, sequence boundaries and transgressive surfaces are more readily identified than maximum flooding surfaces. This is because LSTs in the Tununk Shale show resistant ledges in outcrop (Fig. 7) and the highest amount of storm-generated sedimentary features in each sequence (Figs 4 and 6). The abrupt increase in the abundance and thickness of storm deposits in the LSTs indicates that LSTs were deposited during periods of the shallowest water depth in each sea-level cycle. In the Tununk Shale, the basal sequence boundaries (SBs) of sequences 2 to 4 show minor erosional features such as thin lags of broken shell fragments or erosional bases of centimetre-thick wave ripple laminations, which are interpreted as minor hiatuses resulting from bottom scour by storm events (Schieber, 1998b). Nonetheless, the strata underlying and overlying the SBs are largely conformable. Therefore, in the Tununk Shale, the SBs at the bases of LSTs are interpreted as the correlative conformity developed at the lowest relative point of sea level, *sensu* Hunt & Tucker (1992).

Across the transgressive surfaces (TSs) in all sequences in the Tununk Shale, the abundance and thickness of storm-generated sedimentary features abruptly decreases. Trace-fossil diversity tends to decrease as well, whereas BI increases to some degree in the TST compared to the underlying LST. The retrogradational shift of facies across TSs indicates rising sea level, which results in decreasing frequency and magnitude of storm reworking and lower sedimentation rates, and therefore cumulatively enhances preservation potential of bioturbation features leading to higher BI. All TSs are closely related to intervals that show abrupt increase in carbonate content. For example, the TS of sequence 2 is picked on top of the uppermost laterally continuous wave ripple or combined-flow ripple laminations (the flooding surfaces marked in Fig. 7B and E). Directly below this TS, abundant biogenic carbonate particles were concentrated by winnowing, and subsequently cemented by calcite (Fig. 15B to F). In S3 and S4, sequences that contain an abundance of detrital grains, TSs are also marked by better-cemented layers or carbonate concretion layers (Fig. 20E). The enrichment of early diagenetic minerals indicates intervals of very slow sedimentation or breaks in sedimentation, when microbially driven diagenetic reactions allowed accumulation of calcite cements in pore spaces of surficial sediments (Raiswell, 1988; Raiswell & Fisher, 2000; Aplin & Macquaker, 2011). Such conditions commonly occur close to stratal surfaces and during deposition of condensed sections (Taylor *et al.*, 2000; Macquaker *et al.*, 2007), which is consistent with an abrupt relative rise of sea level across TSs.

Maximum flooding surfaces are more difficult to identify in the Tununk Shale, in part because the intervals around the MFSs tend to be fine-grained, and thus prone to significant weathering that hides these features under debris. The cryptic nature of MFSs in the Mancos Shale (Campanian age) is also noted by Macquaker *et al.* (2007). In this study, maximum flooding surfaces are identified based on several criteria. Firstly, the MFS in each sequence can be determined at the point where parasequence stacking patterns change from retrogradational to progradational or aggradational. Therefore, MFS can be picked at the turnaround point by looking for an increase in average grain size, storm-generated sedimentary features, trace-fossil diversity and burrow size. Secondly, in the lower calcareous part of the Tununk Shale (especially for S1 and S2), the carbonate content derived from primary productivity in the Tununk Shale is primarily controlled by the degree of clastic dilution of the sediment input from primary productivity (coccoliths, foraminifera tests and faecal pellets). Therefore, the MFSs in S1 and S2 are associated with the highest carbonate content derived from primary productivity in each sequence, reflecting minimal clastic dilution at times of maximum relative sea level. Thirdly, features like well-cemented layers, carbonate concretion layers

and concentrations of fossil fragments or phosphatic particles are commonly related to periods of sediment condensation (overall low sedimentation rate or constant winnowing by bottom currents) during the rapid sea-level rise (Kidwell, 1986; Loutit *et al.*, 1988; Macquaker *et al.*, 1996; Taylor & Macquaker, 2014; Li & Schieber, 2015; Föllmi, 2016). These features are particularly useful for identifying maximum flooding surfaces in S3 and S4. Although the TSs and MFSs in the lower carbonate-rich sequences (S1 and S2), as well as in the upper siliciclastic-dominated sequences (S3 and S4), are all associated with intervals that show abrupt increase in carbonate content, it is critical to be cognisant of the fact that carbonate can be derived from different sources (primary input versus diagenetic cementation) and therefore has different implications for the depositional conditions (see next section for a more detailed discussion).

Above the MFSs, HST parasequences in each sequence show an overall up-section increase in the abundance of storm-generated sedimentary features, trace-fossil diversity and burrow size. The progradational stacking pattern of HST parasequences is interpreted as a result of decreasing water-depth, better water oxygenation and increased nutrient/food availability during the general shallowing of sea level and regression in each sequence. In some studies, degradational parasequence sets (forced regression) that follow the normal regression implicit in HSTs have been described as falling-stage system tracts (FSST) (Posamentier *et al.*, 1992; Posamentier & Allen, 1999). The transition from the normal regression of the HST to the forced regression of the FSST is also represented by a correlative conformity (*sensu* Posamentier & Allen, 1999), but whether any of these are present in the Tununk Shale presents a challenge under the best of circumstances and cannot be determined with any degree of certainty from the data collected for this study. Therefore, the FSST is not included here, but it is noted that the overall regressive trend of the HSTs in the Tununk Shale may consist of both normal and forced regressive elements (Figs 4 and 6).

Comparing sedimentological–petrographic with mineralogy based sequence stratigraphic analysis

In an earlier study, based on detailed analyses of grain size (i.e. content of the non-calcareous coarse silt and sand) and mineralogy (i.e. weight percent of carbonate), at least 37 parasequences and six sequences were identified in outcrops of the Tropic Shale along the southern edge of the Kaiparowits Plateau and in the Tununk Shale of the southern Henry Mountains region (Leithold, 1994). The six sequences are described as third-order transgressive–regressive cycles (cycles 1 to 6), within which the MFSs are identified as the most calcareous horizons in each sequence (Leithold, 1994). In general, cycle 3 to cycle 6 identified in Leithold (1994) correspond to sequence 1 to sequence 4 in this study, respectively. In the present study area, cycle 1 and cycle 2 as documented from the Kaiparowits Plateau area are not preserved owing to the disconformity at the base of the Tununk Shale. Despite the overall consistency between Leithold (1994) and this study regarding the third-order sea-level cycles, distinct differences exist between the sequence stratigraphic frameworks of the two studies.

The most distinct difference is the designation of the surface capping the S2 LST in this study. As described before, the LST parasequence of S2, which lies above T5 and has a thickness of 1 to 2 m, is characterized by moderate and low bioturbation intensity in the lower and upper part, respectively (Fig. 13). The same trend in BI is also documented for the 1 to 2 m interval above T5 in Leithold (1994) and Sethi & Leithold (1997). The surface capping this parasequence was previously identified as a MFS based on: (i) the highest weight percent carbonate measured in this sequence; and (ii) minimal BI, which was interpreted to reflect minimum oxygen level (preserved laminae were not disrupted by burrows) during maximum transgression (Leithold, 1994). In this study, with additional observations of sedimentological and petrographic characteristics, the upward decrease in BI is interpreted to be due to higher sedimentation rate, revealed by more abundant and thicker wave ripple and combined-flow ripple laminae upward in the parasequence (Fig. 14A to D). These storm-generated sedimentary structures consist dominantly of silt-sized to sand-sized planktonic foraminifera tests and shell fragments, indicating frequent storm reworking of these carbonate particles as water depth decreased upward within the parasequence. The distinct decrease in these carbonate-dominated wave ripple and combined-flow ripple laminae, as well as the increase in BI, above the uppermost LST parasequence most plausibly indicates an abrupt relative rise of sea level across a TS.

Regarding the highest carbonate content in this sequence, petrographic observations show that these laminae/beds consist dominantly of planktonic foraminifera tests, which are well-cemented by early diagenetic calcite (Fig. 15D to F). Therefore, the heightened carbonate content directly below the TS in S2 is due to the combined effects of depositional reworking and formation of early diagenetic calcite cement. Nonetheless, it is critical to note that the lithological contrast (high carbonate content) had already been produced as a consequence of depositional processes, and that early diagenesis only amplified an already existing lithological contrast. Therefore, although variations in carbonate content in the lower part of the Tununk Shale (especially S1 and S2) can on first approximation be considered as controlled by clastic dilution, other processes such as reworking by storms and early diagenesis can also have a significant impact on the carbonate content.

In the upper part of the Tununk Shale (S3 to S4), the sediment contribution from primary productivity becomes minor to absent. Layers with high carbonate content in this interval are associated mainly with carbonate concretions and better-cemented layers, and lags of fossil and phosphate fragments. All of these features indicate periods of sediment starvation and can be used to interpret significant flooding events (i.e. TS and MFS). However, without the benefit of parasequence stacking patterns inferred from variations in sedimentary facies and bioturbation characteristics, a TS cannot always be distinguished from a MFS unequivocally based solely on increases in the carbonate content. Moreover, in a situation where only a small amount of carbonate is supplied by primary productivity, overall variability in carbonate content is small as well. This circumstance makes the identification of parasequences based on clastic dilution much more challenging. Therefore, mineralogical proxies have to be integrated with detailed analyses of sedimentary facies, bioturbation and petrographic characteristics, in order to construct robust sequence-stratigraphic frameworks in thick mudstone successions.

High-order relative cycles of sea level during Early to Middle Turonian

The Tununk Shale shows systematic facies variations on varying scales. At least 49 parasequences have been identified in the Tununk Shale in all three measured sections. Based on parasequence stacking patterns, they can be grouped into 11 system tracts and four depositional sequences, revealing a hierarchy of stratal cyclicity recorded in the Tununk Shale.

Vertical variations in lithofacies types and sedimentary facies characteristics indicate that the depositional environment of the Tununk Shale shifted laterally from a distal middle-shelf to an outer-shelf (S1 to S2) setting, and then from an outer-shelf to an inner-shelf environment (S2 to S3, then to S4). These lateral shifts were controlled mainly by the second-order Greenhorn transgressive–regressive sea-level cycle (Leithold, 1994). Similar to other long-term sea-level cycles in the Western Interior Seaway (WIS), the Greenhorn second-order sea-level cycle has been attributed to basin-scale tectonic subsidence (Kauffman, 1985; Gardner, 1995) and can be correlated to the long-term eustatic sea-level cycles during the Late Cretaceous (Haq, 2014).

The presence of four sequences in the Tununk Shale of the study area indicates the superposition of higher-order sea-level changes on the second-order Greenhorn cycle. Constrained by bentonite marker beds and the biostratigraphic framework of Early to Middle Turonian times, the sea-level curve interpreted from the sequence stratigraphic framework of the Tununk Shale (Fig. 22) can be compared with the global eustatic curve. Out of the three sequence boundaries in the Tununk Shale, two (basal SBs of S3 and S4) appear to be globally extensive. The basal SB of S3 is located in the uppermost *M. nodosoides* Zone, just below the base of the *C. woollgari* Zone that is commonly used to mark the Lower–Middle Turonian boundary (Fig. 22). A sea level drop (SB) has been identified in the uppermost *M. nodosoides* Zone in many stratigraphic sections worldwide (Sageman, 1996; Jarvis *et al.*, 2006; Wendler *et al.*, 2016, and references therein). The basal SB of S3 appears to be equivalent to KTu2 of Haq (2014). The basal SB of S4 (Fig. 22) can be correlated to a widely recognized and presumably synchronous sea-level drop (SB) in the middle *C. woollgari* Zone of the Middle Turonian (Gale, 1996; Sahagian *et al.*, 1996; Miller *et al.*, 2003; Wendler *et al.*, 2016) and appears to correspond to KTu3 in Haq (2014). The basal SB of S2 in the lower *M. nodosoides* Zone does not appear to correlate with a global sea-level drop, but the possibility of its eustatic nature cannot be entirely excluded from consideration. Unlike the basal SBs of S3 and S4, the basal SB of S2 is

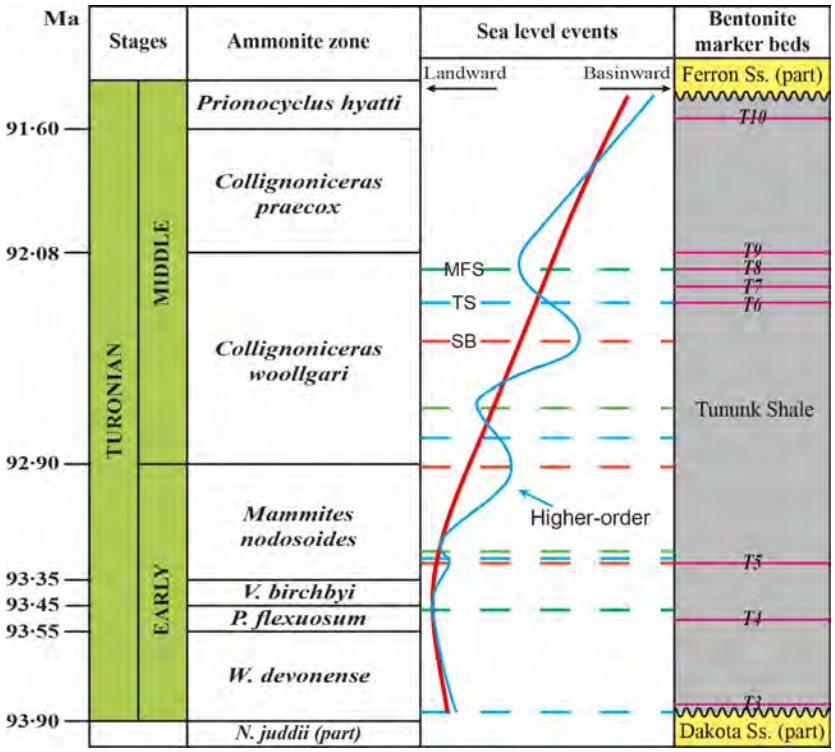

Fig. 22. Interpreted long-term (second-order) and short-term sea-level curves based on the sequence stratigraphic framework of the Tununk Shale developed in this study. The timing of interpreted sea-level events is firstly constrained by their relative stratigraphic positions within bentonite marker beds. The interpreted sea-level curves can then be plotted against the biostratigraphic framework based on the correlation between ammonite biostratigraphy and bentonite marker beds (after Zelt, 1985; Leithold, 1994; Leithold & Dean, 1998). Absolute dates are from Ogg *et al.*, 2012.

only hinted at by subtle changes in sedimentary facies and bioturbation characteristics without any distinct change in lithofacies. Moreover, the small-amplitude relative fall event of sea level suggested by this SB is superimposed on a long-term global sea-level highstand (Fig. 22). In many stratigraphic sections worldwide this time period is represented by fine-grained hemipelagic to pelagic marlstones or chalks (Jarvis *et al.*, 2006; Wendler *et al.*, 2016). Without detailed analysis of their sedimentological and biogenic features, it can be challenging to identify this SB in fine-grained sedimentary successions. Nevertheless, a SB in the lower *M. nodosoides* Zone has been recorded in Pueblo, Colorado (Sageman, 1996), and in southern New Mexico (Mack *et al.*, 2016). Therefore, the basal SB of S2 at least represents a basin-scale event and potentially marks episodic tectonism (for example, changes in rates of thrusting) in the foreland basin.

At least 49 parasequences are documented in the Tununk Shale in this study. The interval between bentonite marker beds T3 and T10 can be used to estimate the average duration of each parasequence because both the base and top of the Tununk Shale are disconformity surfaces that can only be assigned an approximate age. Based on the stratigraphic position of T3 and T10 in the biostratigraphic framework (Fig. 2), a total of 47 parasequences are recorded within a time span of approximately 2·2 Ma. Thus, the average parasequence duration is *ca* 47 kyr. Considering that it is quite plausible that additional thin parasequences may not have been resolved in this study (note the outliers in Fig. 10), the average duration represented by each parasequence could possibly reflect 41 kyr obliquity cycles (Fischer, 1980). Therefore, the short-term cycles recorded by the parasequences in the Tununk Shale are interpreted to be controlled mainly by the obliquity cycle of the Milankovitch frequency band. The effect of climatic changes driven by Milankovitch cycles has been widely documented in the sedimentary records in the WIS (e.g. Fischer *et al.*, 1985; Elder *et al.*, 1994; Sageman *et al.*, 1997, 1998). Nonetheless, the specific mechanism of how the high-frequency facies variations in these rocks were produced by climatic cycles (for example, changes in freshwater runoff, changes in primary productivity or eustatic sea-level changes) remains controversial (Eldrett *et al.*, 2015; Sames *et al.*, 2016; Wendler *et al.*, 2016). To solve this problem requires more case studies examining the complex variability in fine-grained sedimentary rock successions in detail. Careful correlation of the high-frequency facies variations between different depositional environments in

the WIS (for example, siliciclastic-input-dominated versus productivity-dominated settings) and other places around the world is critical to fully unravelling the short-term climate and sea-level changes (if any) during the Late Cretaceous.

CONCLUSION

In this study, sequence stratigraphic concepts have been successfully applied to the thick ancient shelf mudstone succession of the Upper Cretaceous Tununk Shale in south-central Utah. Based on detailed analyses of sedimentary facies, bioturbation and petrographic characteristics, at least 49 parasequences can be identified in the Tununk Shale. Each parasequence shows a coarsening-upward trend that is characterized by upward increases in silt and sand content. Silt-sized/sand-sized particles of both siliciclastic and biogenic origins can be considered as 'detrital' particles because they are both subject to reworking and concentration by bottom currents. In each parasequence, the thickness and lateral continuity of laminae/beds and abundance of storm-generated sedimentary structures increases upward, indicative of a shallowing-upward trend. Based on parasequence stacking patterns, these parasequences collectively can be grouped into 11 system tracts and four sequences, and key sequence stratigraphic surfaces (i.e. sequence boundaries, transgressive surfaces and maximum flooding surfaces) can be identified.

Parasequences in the Tununk Shale show considerable variability, which is mainly due to changes in dominant sediment supply, depositional processes and bioturbation characteristics. Understanding the changes in rock composition and particle origin is a prerequisite for identification of parasequences in different lithofacies types. In the Tununk Shale, changes of lithofacies types are produced by the lateral shift (changing water depth) of depositional environments on a storm-dominated shelf. This study interprets these changes to have been influenced by a hierarchy of eustatic changes within the second-order Greenhorn tectonoeustatic cycle. The presence of four depositional sequences may reflect the superposition of higher-order sea-level changes superimposed on the second-order Greenhorn cycle. Considering the close correlation with global sea-level events, these short-term sea-level cycles recorded in the Tununk Shale appear to be dominantly controlled by eustatic changes. The average duration of parasequences within the Tununk Shale is estimated to be about 40 kyr, strongly suggesting the obliquity-dominated Milankovitch-scale climatic cyclicity.

Sequence stratigraphic analysis allows the prediction of variations in the lithology, sedimentary facies and bioturbation characteristics in the Tununk Shale on the millimetre-scale to metre-scale. The detailed sequence stratigraphic framework developed in this study helps understanding of the underlying causes of multi-scalar variability and heterogeneity in seemingly homogenous thick mudstone successions. The application of sequence-stratigraphic concepts to such strata requires detailed and integrated analyses of grain size, particle origin, sedimentary structures and biogenic features, because only those properties can directly provide critical information regarding the spatial and temporal evolution of the depositional setting of these rocks.

ACKNOWLEDGEMENT

Comments by Kevin Bohacs on an earlier version of the manuscript are greatly appreciated. We thank Massimo Zecchin, Joe Macquaker, Bruce Hart, Associate Editor Massimiliano Ghinassi and Editor Ian Kane for their valuable comments and suggestions on the manuscript. This research was supported by the sponsors of the Indiana University Shale Research Consortium (Anadarko, Chevron, ConocoPhillips, ExxonMobil, Shell, Statoil, Marathon, Whiting and Wintershall). Additional support was provided through student research grants and fellowships awarded to Zhiyang Li by the Geological Society of America, SEPM (Society for Sedimentary Geology), American Association of Petroleum Geologists (Donald A. and Mary O'Nesky Named Grant) and the Indiana University Department of Geological Sciences (Grassman fellowship). Many thanks to Sue Fivecoat and John Reay from the Bureau of Land Management at Henry Mountains Field Station for their guidance and help on granting us permits for fieldwork in the study area. We also thank Bei Liu, Britt Rossman and Matthew Leung for their assistance in the field.

REFERENCES

Abreu, V., **Pederson, K.**, **Neal, J.** and **Bohacs, K.M.** (2014) A simplified guide for sequence stratigraphy: nomenclature, definitions and method (abstract). In: *William Smith Meeting*. Geological Society, London.

Allison, M.A., **Lee, M.T.**, **Ogston, A.S.** and **Aller, R.C.** (2000) Origin of Amazon mudbanks along the northeastern coast of South America. *Mar. Geol.*, **163**, 241–256.

Aplin, A.C. and **Macquaker, J.H.S.** (2011) Mudstone diversity: origin and implications for source, seal, and reservoir properties in petroleum systems. *AAPG Bull.*, **95**, 2031–2059.

Ayranci, K., **Harris, N.B.** and **Dong, T.** (2018) High resolution sequence stratigraphic reconstruction of mud-dominated systems below storm wave base; A case study from the Middle to Upper Devonian Horn River Group, British Columbia, Canada. *Sed. Geol.*, **373**, 239–253.

Barron, E.J. (1989) Severe storms during Earth history. *Geol. Soc. Am. Bull.*, **101**, 601–612.

Bentley, S.J. and **Nittrouer, C.A.** (2003) Emplacement, modification, and preservation of event strata on a flood-dominated continental shelf: Eel shelf, Northern California. *Cont. Shelf Res.*, **23**, 1465–1493.

Birgenheier, L.P., **Horton, B.**, **McCauley, A.D.**, **Johnson, C.L.** and **Kennedy, A.** (2017) A depositional model for offshore deposits of the lower Blue Gate Member, Mancos Shale, Uinta Basin, Utah, USA. *Sedimentology*, **64**, 1402–1438.

Blakey, A.C. (2014) Paleogeography and Paleotectonics of the Western Interior Seaway, Jurassic-Cretaceous of North America. *AAPG Search and Discovery Article #30392*, 1–72.

Bohacs, K.M. (1998) Contrasting expressions of depositional sequences in mudrocks from marine to non marine environs. In: *Shales and Mudstones* (Eds J. Schieber, W. Zimmerle and P.S. Sethi), pp. 33–78. Schweizerbart'sche Verlagsbuchhandlung, Stuttgart.

Bohacs, K.M. and **Schwalbach, J.R.** (1992) Sequence stratigraphy of fine-grained rocks with special reference to the Monterey Formation. In: *Field Trip Guidebook*, *SEPM Pacific Sec.*, **70**, 7–19.

Bohacs, K.M., **Grabowski, G.J., Jr**, **Carroll, A.R.**, **Mankiewicz, P.J.**, **Miskell-Gerhardt, K.J.**, **Schwalbach, J.R.**, **Wegner, M.B.** and **Simo, J.A.** (2005) Production, destruction, and dilution; the many paths to source-rock development. *Spec. Publ. – Soc. Sed. Geol.*, **82**, 61–101.

Bohacs, K.M., **Lazar, O.R.** and **Demko, T.M.** (2014) Parasequence types in shelfal mudstone strata—Quantitative observations of lithofacies and stacking patterns, and conceptual link to modern depositional regimes. *Geology*, **42**, 131–134.

Cattaneo, A., **Correggiari, A.**, **Langone, L.** and **Trincardi, F.** (2003) The late-Holocene Gargano subaqueous delta, Adriatic shelf: sediment pathways and supply fluctuations. *Mar. Geol.*, **193**, 61–91.

Cattaneo, A., **Trincardi, F.**, **Asioli, A.** and **Correggiari, A.** (2007) The Western Adriatic shelf clinoform: energy-limited bottomset. *Cont. Shelf Res.*, **27**, 506–525.

Catuneanu, O. (2006) *Principles of Sequence Stratigraphy*. Elsevier, Amsterdam, 375 pp.

Catuneanu, O., **Abreu, V.**, **Bhattacharya, J.P.**, **Blum, M.D.**, **Dalrymple, R.W.**, **Eriksson, P.G.**, **Fielding, C.R.**, **Fisher, W.L.**, **Galloway, W.E.**, **Gibling, M.R.**, **Giles, K.A.**, **Holbrook, J.M.**, **Jordan, R.**, **Kendall, C.G.S.C.**, **Macurda, B.**, **Martinsen, O.J.**, **Miall, A.D.**, **Neal, J.E.**, **Nummedal, D.**, **Pomar, L.**, **Posamentier, H.W.**, **Pratt, B.R.**, **Sarg, J.F.**, **Shanley, K.W.**, **Steel, R.J.**, **Strasser, A.**, **Tucker, M.E.** and **Winker, C.** (2009) Towards the standardization of sequence stratigraphy. *Earth-Sci. Rev.*, **92**, 1–33.

Catuneanu, O., **Galloway, W.E.**, **Kendall, C.G.S.C.**, **Miall, A.D.**, **Posamentier, H.W.**, **Strasser, A.** and **Tucker, M.E.** (2011) Sequence stratigraphy: methodology and nomenclature. *Newsl. Stratigr.*, **44**, 173–245.

DeCelles, P.G. (2004) Late Jurassic to Eocene evolution of the Cordilleran thrust belt and foreland basin system, western U.S.A. *Am. J. Sci.*, **304**, 105–168.

Eaton, J.G., **Kirkland, J.I.** and **Kauffman, E.G.** (1990) Evidence and dating of Mid-Cretaceous tectonic activity in the San Rafael Swell, Emery County, Utah. *Mt. Geol.*, **27**, 39–45.

Elder, W.P., **Gustason, E.R.** and **Sageman, B.B.** (1994) Correlation of basinal carbonate cycles to nearshore parasequences in the Late Cretaceous Greenhorn seaway, Western Interior U.S.A. *Geol. Soc. Am. Bull.*, **106**, 892–902.

Eldrett, J.S., **Ma, C.**, **Bergman, S.C.**, **Ozkan, A.**, **Minisini, D.**, **Lutz, B.**, **Jackett, S.-J.**, **Macaulay, C.** and **Kelly, A.E.** (2015) Origin of limestone–marlstone cycles: astronomic forcing of organic-rich sedimentary rocks from the Cenomanian to Early Coniacian of the Cretaceous Western Interior Seaway, USA. *Earth Planet. Sci. Lett.*, **423**, 98–113.

Ericksen, M.C. and **Slingerland, R.L.** (1990) Numerical simulations of tidal and wind-driven circulation in the Cretaceous interior seaway of North America. *Geol. Soc. Am. Bull.*, **102**, 1499–1516.

Fischer, A.G. (1980) Gilbert—bedding rhythms and geochronology. In: *The Scientific Ideas of G. K. Gilbert* (Ed E.L. Yochelson), *Geological Society of America Special Papers*, pp. 93–104.

Fischer, A.G., **Herbert, T.** and **Silva, I.P.** (1985) Carbonate bedding cycles in cretaceous pelagic and hemipelagic sequences. In: *Fine-Grained Deposits and Biofacies of the Cretaceous Western Interior Seaway: Evidence of Cyclic Sedimentary Processes* (Eds L.M. Pratt, E.G. Kauffman and F.B. Zelt), pp. 1–10. SEPM Society for Sedimentary Geology, Tulsa.

Föllmi, K.B. (2016) Sedimentary condensation. *Earth-Sci. Rev.*, **152**, 143–180.

Gale, A.S. (1996) Turonian correlation and sequence stratigraphy of the Chalk in southern England. *Geol. Soc. London. Spec. Publ.*, **103**, 177–195.

Gardner, M.H. (1995) Tectonic and eustatic controls on the stratal architecture of mid-Cretaceous stratigraphic sequences, central western interior foreland basin of North America. In: *Stratigraphic Evolution of Foreland Basins* (Eds S.L. Dorobek and G.M. Ross), *SEPM (Society for Sedimentary Geology)***52**, pp. 243–282.

Gardner, M.H. and **Cross, T.A.** (1994) Middle Cretaceous paleogeography of Utah, pp. 471–502. SEPM (Society for Sedimentary Geology), Rocky Mountain Section, Denver, CO.

Haq, B.U. (2014) Cretaceous eustasy revisited. *Global Planet. Change*, **113**, 44–58.

Hart, B.S. (2016) Marine mudstone source rocks in epicontinental basins: development of a conceptual facies model and application to Cenomanian/Turonian mudstones of the Cretaceous Western Interior Seaway. In: *Hydrocarbon Source Rocks in Unconventional Plays, Rocky Mountain Region* (Eds M. Dolan, D. Higley and P. Lillis), *Rocky Mountain Association of Geologists Special Publication*, pp. 1–58.

Hunt, D. and **Tucker, M.E.** (1992) Stranded parasequences and the forced regressive wedge systems tract: deposition during base-level fall. *Sed. Geol.*, **81**, 1–9.

Jarvis, I.A.N., **Gale, A.S.**, **Jenkyns, H.C.** and **Pearce, M.A.** (2006) Secular variation in Late Cretaceous carbon isotopes: a new $\delta^{13}C$ carbonate reference curve for the Cenomanian-Campanian (99.6–70.6 Ma). *Geol. Mag.*, **143**, 561.

Jervey, M.T. (1988) Quantitative geological modeling of siliciclastic rock sequences and their seismic expression. In: *Sea-Level Changes: An Integrated Approach* (Eds C.K. Wilgus, B.S. Hastings, H. Posamentier, J. Van Wagoner, C.A. Ross and C.G.S.C. Kendall), *SEPM Spec. Publ.*, **42**, pp. 47–69.

Kauffman, E.G. (1977) Geological and biological overview: western Interior Cretaceous basin. *Mt. Geol.*, **14**, 75–99.

Kauffman, E.G. (1985) Cretaceous evolution of the Western Interior Basin of the United States. *SEPM Guidebook*, **4**, 4–13.

Kauffman, E.G. and **Caldwell, W.G.E.** (1993) The Western Interior Basin in space and time. *Geol. Assoc. Can. Spec. Pap.*, **39**, 1–30.

Kidwell, S.M. (1986) Models for fossil concentrations: paleobiologic implications. *Paleobiology*, **12**, 6–24.

Kineke, G.C., **Sternberg, R.W.**, **Trowbridge, J.H.** and **Geyer, W.R.** (1996) Fluid-mud processes on the Amazon continental shelf. *Cont. Shelf Res.*, **16**, 667–696.

Kuehl, S.A., **DeMaster, D.J.** and **Nittrouer, C.A.** (1986) Nature of sediment accumulation on the Amazon continental shelf. *Cont. Shelf Res.*, **6**, 209–225.

Lazar, O.R., **Bohacs, K.M.**, **Schieber, J.**, **Macquaker, J.H.S.** and **Demko, T.M.** (2015) *Mudstone Primer*. SEPM Society for Sedimentary Geology, 205 pp.

Leithold, E.L. (1994) Stratigraphical architecture at the muddy margin of the Cretaceous Western Interior Seaway, southern Utah. *Sedimentology*, **41**, 521–542.

Leithold, E.L. and **Dean, W.E.** (1998) Depositional processes and carbon burial on a Turonian prodelta at the margin of the Western Interior Seaway. *Concepts Sed. Paleontol.*, **6**, 189–200.

Li, Y. and **Schieber, J.** (2015) On the origin of a phosphate enriched interval in the Chattanooga Shale (Upper Devonian) of Tennessee—A combined sedimentologic, petrographic, and geochemical study. *Sed. Geol.*, **329**, 40–61.

Li, Z. and **Schieber, J.** (2018a) Detailed facies analysis of the Upper Cretaceous Tununk Shale Member, Henry Mountains Region, Utah: implications for mudstone depositional models in epicontinental seas. *Sed. Geol.*, **364**, 141–159.

Li, Z. and **Schieber, J.** (2018b) Composite Particles in Mudstones: examples from the Late Cretaceous Tununk Shale Member of the Mancos Shale Formation. *J. Sed. Res.*, **88**, 1319–1344.

Li, Z., **Bhattacharya, J.** and **Schieber, J.** (2015) Evaluating along-strike variation using thin-bedded facies analysis, Upper Cretaceous Ferron Notom Delta, Utah. *Sedimentology*, **62**, 2060–2089.

Liu, J.P., **Xu, K.H.**, **Li, A.C.**, **Milliman, J.D.**, **Velozzi, D.M.**, **Xiao, S.B.** and **Yang, Z.S.** (2007) Flux and fate of Yangtze River sediment delivered to the East China Sea. *Geomorphology*, **85**, 208–224.

Liu, S., **Nummedal, D.** and **Liu, L.** (2011) Migration of dynamic subsidence across the Late Cretaceous United States Western Interior Basin in response to Farallon plate subduction. *Geology*, **39**, 555–558.

Livaccari, R.F. (1991) Role of crustal thickening and extensional collapse in the tectonic evolution of the Sevier-Laramide orogeny, western United States. *Geology*, **19**, 1104–1107.

Loutit, T.S., **Hardenbol, J.**, **Vail, P.R.** and **Baum, G.R.** (1988) Condensed sections: the key to age determination and correlation of continental margin sequences. In: *Sea Level Change and Integrated Approach* (Eds C. Wilgus, B.S. Hastings, C.G.S.C. Kendall, H.W. Posamentier, C.A. Ross and V.W.J. C), *SEPM Spec. Publ.*, **42**,183–216.

MacEachern, J.A., **Bann, K.L.**, **Bhattacharya, J.P.** and **Howell, C.D., Jr** (2005) Ichnology of deltas; organism responses to the dynamic interplay of rivers, waves, storms, and tides. *SEPM Spec. Publ.*, **83**, 49–85.

MacEachern, J.A., **Bann, K.L.**, **Pemberton, S.G.** and **Gingras, M.K.** (2007) The ichnofacies paradigm: high-resolution paleoenvironmental interpretation of the rock record. In: *Applied Ichonology, SEPM Short Course Notes 52* (Eds J.A. MacEachern, K.L. Bann, M.K. Gingras and S.G. Pemberton), pp. 27–64. SEPM, Tulsa, OK.

Mack, G.H., **Hook, S.**, **Giles, K.A.** and **Cobban, W.A.** (2016) Sequence stratigraphy of the Mancos Shale, lower Tres Hermanos Formation, and coeval Middle Cenomanian to middle Turonian strata, southern New Mexico, USA. *Sedimentology*, **63**, 781–808.

Macquaker, J.H.S. and **Howell, J.K.** (1999) Small-scale (<5.0 m) vertical heterogeneity in mudstones: implications for high-resolution stratigraphy in siliciclastic mudstone successions. *J. Geol. Soc.*, **156**, 105–112.

Macquaker, J.H.S. and **Taylor, K.G.** (1996) A sequence-stratigraphic interpretation of a mudstone-dominated succession: the Lower Jurassic Cleveland Ironstone Formation, UK. *J. Geol. Soc.*, **153**, 759.

Macquaker, J.H.S., **Taylor, K.G.**, **Young, T.P.** and **Curtis, C.D.** (1996) Sedimentological and geochemical controls on ooidal ironstone and 'bone-bed' formation and some comments on their sequence-stratigraphical significance. In: *Sequence Stratigraphy in British Geology* (Eds S.P. Hesselbo and D.N. Parkinson), *Geol. Soc. Spec. Publ.*, **103**, 97–107.

Macquaker, J.H.S., **Gawthorpe, R.L.**, **Taylor, K.G.** and **Oates, M.J.** (1998) Heterogeneity, stacking patterns and sequence stratigraphic interpretation in distal mudstone successions; examples from the Kimmeridge Clay Formation, U.K, pp. 163–186. E. Schweizerbart'sche Verlagsbuchhandlung Naegele u. Obermiller, Stuttgart, Federal Republic of Germany, Germany.

Macquaker, J.H.S., **Taylor, K.G.** and **Gawthorpe, R.L.** (2007) High-Resolution Facies Analyses of Mudstones: implications for Paleoenvironmental and Sequence Stratigraphic Interpretations of Offshore Ancient Mud-Dominated Successions. *J. Sed. Res.*, **77**, 324–339.

Miller, K.G., **Sugarman, P.J.**, **Browning, J.V.**, **Kominz, M.A.**, **Hernández, J.C.**, **Olsson, R.K.**, **Wright, J.D.**, **Feigenson, M.D.** and **Van Sickel, W.** (2003) Late Cretaceous chronology of large, rapid sea-level changes: glacioeustasy during the greenhouse world. *Geology*, **31**, 585–588.

Minoura, K. and **Osaka, Y.** (1992) Sediments and sedimentary processes in Mutsu Bay, Japan: Pelletization as the most important mode in depositing argillaceous sediments. *Mar. Geol.*, **103**, 487–502.

Mitchum, R.M. and **Van Wagoner, J.C.** (1991) High-frequency sequences and their stacking patterns: sequence-stratigraphic evidence of high-frequency eustatic cycles. *Sed. Geol.*, **70**, 131–160.

Nittrouer, C.A., **Kuehl, S.A.**, **DeMaster, D.J.** and **Kowsmann, R.O.** (1986) The deltaic nature of Amazon shelf sedimentation. *Geol. Soc. Am. Bull.*, **97**, 444–458.

Nowell, A.R.M., **Jumars, P.A.** and **Eckman, J.E.** (1981) Effects of biological activity on the entrainment of marine sediments. *Mar. Geol.*, **42**, 133–153.

Oehmig, R. (1993) Entrainment of planktonic foraminifera: effect of bulk density. *Sedimentology*, **40**, 869–877.

Ogg, J.G., **Hinnov, L.A.** and **Huang, C.** (2012) Chapter 27 – Cretaceous. In: *The Geologic Time Scale* (Eds F.M. Gradstein, J.G. Ogg, M.D. Schmitz and G.M. Ogg), pp. 793–853. Elsevier, Boston, MA.

Patruno, S., **Hampson, G.J.** and **Jackson, C.A.L.** (2015) Quantitative characterisation of deltaic and subaqueous clinoforms. *Earth-Sci. Rev.*, **142**, 79–119.

Peterson, F., **Ryder, R.T.** and **Law, B.E.** (1980) Stratigraphy, sedimentology, and regional relationships of the Cretaceous System in the Henry Mountains region, Utah. *Utah Geol. Assoc. Publ.*, 151–170.

Posamentier, H.W. and **Allen, G.P.** (1999) Siliciclastic sequence stratigraphy: concepts and applications. *SEPM Concepts in Sedimentology and Palaeontology*, **7**, 216 pp.

Posamentier, H.W., **Jervey, M.T.** and **Vail, P.R.** (1988) *Eustatic Controls on Clastic Deposition; I, Conceptual Framework*. In: *TSea-Level Changes: an Integrated Approach* (Eds C.K. Wilgus, B.S. Hastings, C.G.S.C. Kendall, H.W. Posamentier, C.A. Ross and J.C. Van Wagoner), Spec. Publ. Soc. *econ. Paleont. Miner*, **42**, pp. 109–124.

Posamentier, H.W., **Allen, G.P.**, **James, D.P.** and **Tesson, M.** (1992) Forced regressions in a sequence stratigraphic framework: concepts, examples, and exploration significance. *AAPG Bull.*, **76**, 1687–1709.

Potter, P.E., **Maynard, J.B.** and **Depetris, P.J.** (2005) *Mud and Mudstones: Introduction and Overview*. Springer-Verlag, Berlin and Heidelberg, 297 pp.

Raiswell, R. (1988) Evidence for surface reaction-controlled growth of carbonate concretions in shales. *Sedimentology*, **35**, 571–575.

Raiswell, R. and **Fisher, Q.J.** (2000) Mudrock-hosted carbonate concretions: a review of growth mechanisms and their influence on chemical and isotopic composition. *J. Geol. Soc.*, **157**, 239–251.

Reynolds, A.D. (2009) Paralic successions. In: *Sequence Stratigraphy* (Eds D. Emery and K. Myers), pp. 134–177. Blackwell Publishing Ltd, Oxford.

Rine, J.M. and **Ginsburg, R.N.** (1985) Depositional facies of a mud shoreface in Suriname, South America; a mud analogue to sandy, shallow-marine deposits. *J. Sed. Res.*, **55**, 633–652.

Ryer, T. and **Lovekin, J.** (1986) The Upper Cretaceous Vernal Delta of Utah—depositional or paleotectonic feature. In: *Paleotectonics and Sedimentation in the Rocky Mountain Region, United States: Part III* (Ed J.A. Peterson), *American Association of Petroleum Geologists Memoir*, **41**, pp. 497–509.

Sageman, B.B. (1996) Lowstand tempestites: depositional model for Cretaceous skeletal limestones, Western Interior basin. *Geology*, **24**, 888–892.

Sageman, B.B. and **Arthur, M.A.** (1994) Early Turonian paleogeographic/paleobathymetric map, Western Interior, U.S. In: *Mesozoic Systems of the Rocky Mountain Region* (Eds M. Caputo and J. Peterson), *Rocky Mountain Section, SEPM Spec. Publ.*, pp. 457–470.

Sageman, B.B., **Rich, J.**, **Arthur, M.A.**, **Birchfield, G.E.** and **Dean, W.E.** (1997) Evidence for Milankovitch periodicities in Cenomanian-Turonian lithologic and geochemical cycles, Western Interior U.S.A. *J. Sed. Res.*, **67**, 286–302.

Sageman, B.B., **Rich, J.**, **Arthur, M.A.**, **Dean, W.E.**, **Savrda, C.E.** and **Bralower, T.J.** (1998) Multiple Milankovitch cycles in the Bridge Creek Limestone (Cenomanian-Turonian), Western Interior Basin. *Concepts Sed. Paleontol.*, **6**, 153–171.

Sahagian, D., **Pinous, O.**, **Olferiev, A.** and **Zakharov, V.** (1996) Eustatic curve for the Middle Jurassic-Cretaceous based on Russian platform and Siberian stratigraphy: zonal resolution. *AAPG Bull.*, **80**, 1433–1458.

Sames, B., **Wagreich, M.**, **Wendler, J.E.**, **Haq, B.U.**, **Conrad, C.P.**, **Melinte-Dobrinescu, M.C.**, **Hu, X.**, **Wendler, I.**, **Wolfgring, E.**, **Yilmaz, I.Ö.** and **Zorina, S.O.** (2016) Review: short-term sea-level changes in a greenhouse world — A view from the Cretaceous. *Palaeogeogr. Palaeoclimatol. Palaeoecol.*, **441**, 393–411.

Savrda, C.E. and **Bottjer, D.J.** (1991) Oxygen-related biofacies in marine strata: an overview and update. *Geol. Soc. London. Spec. Publ.*, **58**, 201–219.

Schieber, J. (1998a) Developing a sequence stratigraphic framework for the Late Devonian Chattanooga Shale of the Southeastern U.S.A.; relevance for the Bakken Shale. *Spec. Publ. – Saskatchewan Geol. Soc.*, **13**, 58–68.

Schieber, J. (1998b) Sedimentary features indicating erosion, condensation, and hiatuses in the Chattanooga Shale of central Tennessee: relevance for sedimentary and stratigraphic evolution. In: *Shales and Mudstones* (Eds J. Schieber, W. Zimmerle and P.S. Sethi), pp. 187–215. E. Schweizerbart'sche Verlagsbuchhandlung, Stuttgart.

Schieber, J. (2011) Reverse engineering mother nature — Shale sedimentology from an experimental perspective. *Sed. Geol.*, **238**, 1–22.

Schieber, J. and **Southard, J.B.** (2009) Bedload transport of mud by floccule ripples—Direct observation of ripple migration processes and their implications. *Geology*, **37**, 483–486.

Schieber, J. and **Zimmerle, W.** (1998) Introduction and overview; the history and promise of shale research. In: *Shales and Mudstones (vol. 1): Basin Studies, Sedimentology and Paleontology* (Eds J. Schieber, W. Zimmerle and P.S. Sethi), pp. 1–10. Schweizerbart'sche, Verlagsbuchhandlung, Stuttgart.

Schieber, J., **Southard, J.** and **Thaisen, K.** (2007) Accretion of mudstone beds from migrating floccule ripples. *Science*, **318**, 1760–1763.

Schieber, J., **Lazar, R.**, **Bohacs, K.**, **Klimentidis, R.**, **Dumitrescu, M.** and **Ottmann, J.** (2016) An SEM study of porosity in the eagle ford shale of Texas—pore types and porosity distribution in a depositional and sequence-stratigraphic context. In: *The Eagle Ford Shale: A Renaissance in U.S. Oil Production* (Ed J. Breyer). *American Association of Petroleum Geologists*, **110**, 167–186.

Sethi, P.S. and **Leithold, E.L.** (1997) Recurrent depletion of benthic oxygen with 4th-order transgressive maxima in the Cretaceous Western Interior Seaway. *Palaeogeogr. Palaeoclimatol. Palaeoecol.*, **128**, 39–61.

Slingerland, R. and **Keen, T.R.** (1999) Sediment transport in the Western Interior Seaway of North America; predictions from a climate-ocean-sediment model. In: *Isolated Shallow Marine Sand Bodies* (Eds K.M. Bergman and J.W. Snedden), *SEPM Spec. Publ.*, **64**, 179–190.

Taylor, A.M. and **Goldring, R.** (1993) Description and analysis of bioturbation and ichnofabric. *J. Geol. Soc. London*, **150**, 141–148.

Taylor, K.G. and **Macquaker, J.H.S.** (2014) Diagenetic alterations in a silt- and clay-rich mudstone succession: an example from the Upper Cretaceous Mancos Shale of Utah, USA. *Clay Mineral.*, **49**, 213–227.

Taylor, K.G., **Gawthorpe, R.L.**, **Curtis, C.D.**, **Marshall, J.D.** and **Awwiller, D.N.** (2000) Carbonate Cementation in a Sequence-Stratigraphic Framework: upper Cretaceous Sandstones, Book Cliffs, Utah-Colorado. *J. Sed. Res.*, **70**, 360–372.

Traykovski, P., **Geyer, W.R.**, **Irish, J.D.** and **Lynch, J.F.** (2000) The role of wave-induced density-driven fluid mud flows for cross-shelf transport on the Eel River continental shelf. *Cont. Shelf Res.*, **20**, 2113–2140.

Vail, P.R. (1987) Seismic stratigraphy interpretation using sequence stratigraphy; Part 1: seismic stratigraphy interpretation procedure. In: *Atlas of Seismic Stratigraphy*, (Ed. A.W. Bally), *AAPG Studies in Geology*, **27**, 1–10.

Van Wagoner, J.C., **Mitchum, R.M., Jr**, **Posamentier, H.W.** and **Vail, P.R.** (1987) Seismic stratigraphy interpretation using sequence stratigraphy; Part 2: key definitions of sequence stratigraphy. In: *Atlas of Seismic Stratigraphy*, (Ed. A.W. Bally), *AAPG Studies in Geology*, **27**, pp. 11–14.

Van Wagoner, J.C., **Posamentier, H.W.**, **Mitchum, R.M., Jr**, **Vail, P.R.**, **Sarg, J.F.**, **Loutit, T.S.** and **Hardenbol, J.** (1988) An overview of the fundamentals of sequence stratigraphy and key definitions. *SEPM Spec. Publ.*, **42**, 39–45.

Van Wagoner, J.C., **Van Mitchum, R.M.**, **Campion, K.M.** and **Rahmanian, V.D.** (1990) *Siliciclastic Sequence Stratigraphy in Well Logs, Cores, and Outcrops*. American Association of Petroleum Geologists, Tulsa, OK, 74 pp.

Ver Straeten, C.A., **Brett, C.E.** and **Sageman, B.B.** (2011) Mudrock sequence stratigraphy: a multi-proxy (sedimentological, paleobiological and geochemical) approach, Devonian Appalachian Basin. *Palaeogeogr. Palaeoclimatol. Palaeoecol.*, **304**, 54–73.

Weimer, R.J. (1984) Relation of unconformities, tectonics, and sea-level changes, Cretaceous of Western Interior, U.S.A. In: *Interregional Unconformities and Hydrocarbon Accumulation* (Ed. J.S. Schlee), **36**, pp. 7–35. American Association of Petroleum Geologists, Tulsa, OK.

Wendler, I., **Wendler, J.E.** and **Clarke, L.J.** (2016) Sea-level reconstruction for Turonian sediments from Tanzania based on integration of sedimentology, microfacies, geochemistry and micropaleontology. *Palaeogeogr. Palaeoclimatol. Palaeoecol.*, **441**, 528–564.

Wheatcroft, R.A. and **Drake, D.E.** (2003) Post-depositional alteration and preservation of sedimentary event layers on continental margins, I. The role of episodic sedimentation. *Mar. Geol.*, **199**, 123–137.

Williams, C.J., **Hesselbo, S.P.**, **Jenkyns, H.C.** and **Morgans-Bell, H.S.** (2001) Quartz silt in mudrocks as a key to sequence stratigraphy (Kimmeridge Clay Formation, Late Jurassic, Wessex Basin, UK). *Terra Nova*, **13**, 449–455.

Wilson, R.D. and **Schieber, J.** (2017) Association Between Wave- and Current-aided Hyperpycnites and Flooding Surfaces in shelfal mudstones: an Integrated Sedimentologic, Sequence Stratigraphic, and Geochemical Approach. *J. Sed. Res.*, **87**, 1143–1155.

Wright, L.D., **Wiseman, W.J.**, **Bornhold, B.D.**, **Prior, D.B.**, **Suhayda, J.N.**, **Keller, G.H.**, **Yang, Z.S.** and **Fan, Y.B.** (1988) Marine dispersal and deposition of Yellow River silts by gravity-driven underflows. *Nature*, **332**, 629–632.

Yonkee, W.A. and **Weil, A.B.** (2015) Tectonic evolution of the Sevier and Laramide belts within the North American Cordillera orogenic system. *Earth-Sci. Rev.*, **150**, 531–593.

Zelt, F.B. (1985) *Natural Gamma-Ray Spectrometry, Lithofacies, and Depositional Environments of Selected Upper Cretaceous Marine Mudrocks, Western United States, Including Tropic Shale and Tununk Member of Mancos Shale*. Princeton University, Princeton, NJ, 372 pp.

Manuscript received 28 August 2018; revision accepted 14 May 2019